The Astrophysical Journal, 856:92 (16pp), 2018 April 1 https://doi.org/10.3847/1538-4357/aab368

Gravitational Waves and Intermediate-mass Black Hole Retention in Globular Clusters

Giacomo Fragione[1], Idan Ginsburg[2], and Bence Kocsis[3]
[1] Racah Institute for Physics, The Hebrew University, Jerusalem 91904, Israel
[2] Astronomy Department, Harvard University, 60 Garden St., Cambridge, MA 02138, USA
[3] Institute of Physics, Eötvös University, Pázmány P. s. 1/A, Budapest, 1117, Hungary
Received 2017 November 2; revised 2018 February 27; accepted 2018 February 27; published 2018 March 28

Abstract

The recent discovery of gravitational waves (GWs) has opened new horizons for physics. Current and upcoming missions, such as LIGO, VIRGO, KAGRA, and *LISA*, promise to shed light on black holes of every size from stellar mass (SBH) sizes up to supermassive black holes. The intermediate-mass black hole (IMBH) family has not been detected beyond any reasonable doubt. Recent analyses suggest observational evidence for the presence of IMBHs in the centers of two Galactic globular clusters (GCs). In this paper, we investigate the possibility that GCs were born with a central IMBH, which undergoes repeated merger events with SBHs in the cluster core. By means of a semi-analytical method, we follow the evolution of the primordial cluster population in the galactic potential and the mergers of the binary IMBH-SBH systems. Our models predict ≈1000 IMBHs within 1 kpc from the galactic center and show that the IMBH-SBH merger rate density changes from $\mathcal{R} \approx 1000\,\mathrm{Gpc^{-3}\,yr^{-1}}$ beyond $z \approx 2$ to $\mathcal{R} \approx$ 1–10 $\mathrm{Gpc^{-3}\,yr^{-1}}$ at $z \approx 0$. The rates at low redshifts may be significantly higher if young massive star clusters host IMBHs. The merger rates are dominated by IMBHs with masses between 10^3 and $10^4\,M_\odot$. Currently, there are no LIGO/VIRGO upper limits for GW sources in this mass range, but our results show that at design sensitivity, these instruments will detect IMBH-SBH mergers in the coming years. *LISA* and the Einstein Telescope will be best suited to detect these events. The inspirals of IMBH-SBH systems may also generate an unresolved GW background.

Key words: galaxies: star clusters: general – Galaxy: kinematics and dynamics – stars: black holes – stars: kinematics and dynamics

1. Introduction

Unlike supermassive (SMBHs; $M \gtrsim 10^5\,M_\odot$) and stellar-mass black holes (SBHs; $10\,M_\odot \lesssim M \lesssim 100\,M_\odot$), the existence of intermediate-mass black holes (IMBHs), with masses $100\,M_\odot \lesssim M \lesssim 10^5\,M_\odot$, has not yet been confirmed. Assuming that the correlation between SMBHs and their stellar environments also holds for the range of IMBH masses (Merritt & Ferrarese 2001; Kruijssen & Lützgendorf 2013; Lützgendorf et al. 2013b; Merritt 2013), such compact objects may be hosted by globular clusters (GCs). Recently, Baumgardt (2017) suggested that ω Cen should host an ≈40,000 $M_\odot$ IMBH in its center, while Kızıltan et al. (2017) showed indirect evidence of an ≈2200 $M_\odot$ IMBH in 47 Tuc. An IMBH would remain dark if not emitting due to accretion. Some pointlike ultraluminous X-ray (ULX) sources ($10^{39} \lesssim L_X/\mathrm{erg\,s^{-1}} \lesssim 10^{41}$) in nearby galaxies are seen to be brighter than typical accreting SBHs but less luminous than typical active galactic nuclei and could be explained by IMBHs (Fabbiano 2006; Davis et al. 2011). In some of these cases, the empirical mass scaling relations of quasi-periodic oscillations also hint at IMBH masses (Abramowicz et al. 2004; Pasham et al. 2014; Kaaret et al. 2017). If present, an IMBH gravitationally interacts with the host cluster and influences the evolution of the GC composition (Baumgardt 2017). However, no direct compelling dynamical evidence of IMBHs has been found to date. In future observations, the IMBHs' dynamical effects and/or their nHz-frequency gravitational waves (GWs) may be indirectly detected in the Milky Way's central nuclear star cluster (Gualandris & Merritt 2009; Gualandris et al. 2010; Kocsis et al. 2012; Merritt 2013). Further, IMBHs may also be detected indirectly in the Milky Way's GCs. The innermost central regions of GCs have not been resolved with sufficient precision to detect IMBHs. The accurate modeling of how IMBHs modify the stellar composition of GCs would facilitate GC-target selection for upcoming surveys (Lützgendorf et al. 2012, 2013a; Mezcua 2017).

One avenue for the formation of IMBHs requires very dense environments as in the centers of GCs. Portegies Zwart & McMillan (2002) found that star clusters with small initial half-mass relaxation times are dominated by stellar collisions driven by the segregation of the most massive stars to the cluster center, where they form hard binaries. The majority of collisions occur with the same star, resulting in the runaway growth of a supermassive object, which may grow up to 0.1% of the mass of the entire star cluster. Similarly, Freitag et al. (2006) showed that in less than the main-sequence lifetime of massive stars (≲3 Myr), a single very massive star can grow up to ≈400–4000 $M_\odot$ through a runaway sequence of mergers. Miller & Hamilton (2002) suggested that IMBHs can form from repeated mergers of an ≈50 $M_\odot$ BH with other SBHs (of lower mass) in the center of a GC. Recently, Giersz et al. (2015) found slow and fast regimes of IMBH mass growth. The larger the initial cluster concentration, the larger the probability of forming an IMBH, which forms earlier and faster. IMBHs may also be produced in the early universe by the direct collapse of massive Pop III stars (Madau & Rees 2001; Whalen & Fryer 2012; Woods et al. 2017), fragmentation of SMBH accretion disks (McKernan et al. 2012, 2014), or super-Eddington accretion of SBHs in SMBH accretion disks (Kocsis et al. 2011). Further, the Milky Way hosts a number of very dense young star clusters in the inner few parsecs, which might form IMBHs as described above (Merritt 2013). The cluster may spiral into the nucleus, carrying the IMBH toward the SMBH until two black holes form a binary system (Fragione et al. 2017;

Petts & Gualandris 2017), also generating bursts of hypervelocity stars (Capuzzo-Dolcetta & Fragione 2015; Fragione & Capuzzo-Dolcetta 2016; Fragione & Ginsburg 2017; Fragione & Gualandris 2018). However, there is currently no compelling evidence of the presence of an IMBH in the galactic center (Merritt 2013), where a cusp of stars is observed (Fragione & Sari 2018).

Several attempts have been done in modeling GCs with IMBHs. Baumgardt (2017) ran a large number of N-body simulations with different mass fractions $M_{\rm BH}/M_{\rm GC}$ of the central IMBH and found indirect evidence that ω Cen could host an IMBH in its center. Lützgendorf et al. (2013) performed N-body simulations of GCs hosting IMBHs, paying attention to the SBH retention fraction and the primordial stellar binary fraction. They found that a cluster with a central IMBH usually has a shorter lifetime as a consequence of the enhanced ejection of stars due to lower mass segregation. MacLeod et al. (2016) investigated the features of the stars and compact remnants bound tightly to the IMBH across the cluster lifetime. Leigh et al. (2014) studied the coexistence of SBH binaries in GCs with a central IMBH. Moreover, SBHs formed from the most massive progenitors could have been embedded in a gas-rich environment for many Myr, which can affect the BH mass distribution and dynamics (Leigh et al. 2013).

GW astronomy will help in the hunt for the first direct evidence of IMBHs. IMBH-SBH binaries may form in GCs and represent a downscaled version of extreme mass-ratio inspirals, the inspiral of a stellar BH into an SMBH (Hopman & Alexander 2006; Amaro-Seoane et al. 2007). LIGO,[4] the Einstein Telescope[5] (ET), and *LISA*[6] will be able to detect IMBH-SBH binaries of different total masses (small, intermediate, and massive, respectively; Amaro-Seoane & Santamaría 2010; Amaro-Seoane et al. 2010). After an IMBH-BH binary forms in a GC, it may produce an IMBH-SBH merger. Mandel et al. (2008) called such events intermediate-mass-ratio inspirals (IMRIs). When BHs merge as a consequence of GW emission, the merger product will be imparted a GW recoil kick, which, depending on the symmetric mass ratio $\eta = q/(1+q)^2$ and spins (here q is the BH mass ratio) of the individual BHs, may be up to several thousands of km s^{-1} times η^2 (Lousto & Zlochower 2011). Due to the small η of an IMRI, such recoils may in many cases not be large enough to expel the IMBH from the cluster. However, Holley-Bockelmann et al. (2008) showed that there is a significant problem in retaining low-mass IMBHs in the merger-rich environment of GCs. They computed that only three of the Milky Way's GCs can retain an IMBH with a mass of 200 $M_\odot$, while around 60 GCs would retain IMBHs with an initial mass of 1000 $M_\odot$. Konstantinidis et al. (2013) found an IMRI in one of their simulations, which led to a merger with a recoil velocity higher than the escape velocity of their simulated GC. Thus, besides forming an IMBH, the challenge is also to retain it inside a star cluster as a consequence of the repeated GW kicks following IMBH-SBH mergers.

In this paper, we address the question of whether the primordial population of GCs that formed in Milky Way–like galaxies can retain their IMBHs and examine the expected distribution of such IMBHs within their host galaxies. In the Milky Way, a few percent of the stars were born in ≈7000 primordial GCs (Gnedin et al. 2014). Even if a small fraction of such GCs hosted IMBHs, the number of IMRIs may be important for GW astronomy and could shed light on the origin and evolution of IMBHs. To do that, we model the evolution of GCs in the Galactic field along with the dynamics of the subcluster of IMBHs and SBHs that form in the cluster core. We use a semi-analytical method to follow the evolution of GCs within the host galaxy (Gnedin et al. 2014) and a Monte Carlo method to follow the evolution of the IMBH within the GC. We account for binary formation via dynamical interactions with stellar encounters, GW emission, and general relativistic recoil kicks and track the evolution of the spin magnitude and direction. While simulations of star clusters with IMBH-SBH coalescences have generally excessive computational costs (Gültekin et al. 2004; Konstantinidis et al. 2013; Leigh et al. 2014), our semi-analytical method allows us to self-consistently model and study the dynamical evolution of the subcluster of IMBHs and SBHs embedded in thousands of primordial GCs while they lose mass and sink toward the galactic center on cosmic timescales.

The paper is organized as follows. In Section 2, we present the semi-analytical method we use to evolve the primordial GC population on cosmic timescales. In Section 3, we analyze the typical dynamics of the subcluster of IMBH and SBHs. We describe our numerical setup in Section 4 and present our results in Section 5. In Section 6, we present our predictions for the rate of IMBH-SBH merger events. Finally, in Section 7, we draw our conclusions.

2. GC Evolution

We discuss the equations used for evolving the GC population (for details, see Gnedin et al. 2014 and references therein). We assume that the cluster formation rate was a fixed fraction $f_{{\rm GC},i}$ of the overall star formation rate,

$$\frac{dM_{\rm GC}}{dt} = f_{{\rm GC},i}\frac{dM_*}{dt}. \quad (1)$$

We set $f_{{\rm GC},i} = 0.011$. We assume that clusters formed at redshift $z = 3$ and calculate their evolution for 11.5 Gyr until today (Gnedin et al. 2014). The initial mass of the clusters is drawn from a power-law distribution

$$\frac{dN_{\rm GC}}{dM_{\rm GC}} \propto M_{\rm GC}^{-\beta}, \quad M_{\rm min} < M < M_{\rm max}. \quad (2)$$

We adopt $\beta = 2$, $M_{\rm min} = 10^4\ M_\odot$, and $M_{\rm max} = 10^7\ M_\odot$. Results do not depend on the choice of $M_{\rm min}$, since light clusters are expected to be disrupted by the Galactic tidal field, and only slightly on the choice of $M_{\rm max}$ (Gnedin et al. 2014).

After formation, GCs lose mass via three mechanisms, i.e., stellar winds, dynamical ejection of stars through two-body relaxation, and removing stars by the galactic tidal field.[7] Following Prieto & Gnedin (2008) and Gnedin et al. (2014), we model the stellar mass loss considering Kroupa (2001) initial mass function and using the main-sequence lifetimes from Hurley et al. (2000) and the stellar remnant masses from Chernoff & Weinberg (1990). We take into account the mass loss due to two-body relaxation and stripping by the galactic

[4] http://www.ligo.org
[5] http://www.et-gw.eu
[6] https://lisa.nasa.gov

[7] The last two mechanisms are not completely independent, since it is two-body relaxation that pushes stars across the tidal boundary. Anyway, when the GC goes deep in the galactic potential, the stripping will be the dominant process.

tidal field according to

$$\frac{dM}{dt} = -\frac{M}{\min(t_{\rm tid}, t_{\rm iso})}, \quad (3)$$

where

$$t_{\rm tid}(r, M) \approx 10\left(\frac{M}{10^5\ M_\odot}\right)^{\alpha} P(r)\ {\rm Gyr} \quad (4)$$

is the typical tidal disruption time (Gieles & Baumgardt 2008) and

$$P(r) = 41.4\left(\frac{r}{\rm kpc}\right)\left(\frac{V_{\rm c}(r)}{\rm km\ s^{-1}}\right)^{-1} \quad (5)$$

is the normalized rotational period of the cluster orbit, which takes into account the strength of the local Galactic field, and $V_{\rm c}(r)$ is the circular velocity at a distance r from the galactic center. We assume $\alpha = 2/3$ (Gieles & Baumgardt 2008; Gnedin et al. 2014). In case of a strong tidal field ($t_{\rm tid} < t_{\rm iso}$), the loss of stars is dominated by the Galactic tidal stripping, while in the limit of a weak tidal field ($t_{\rm tid} > t_{\rm iso}$), the evaporation of stars is controlled by internal dynamics. We compute the evaporation time in isolation as a multiple of the half-mass relaxation time (Gieles et al. 2011; Gnedin et al. 2014),

$$t_{\rm iso}(M) \approx 17\left(\frac{M}{2\times 10^5\ M_\odot}\right)\ {\rm Gyr}. \quad (6)$$

When a cluster arrives near the galactic center, the tidal forces may be strong enough to tear the cluster apart, which happens when the stellar density at a characteristic place in the cluster, such as the core or half-mass radius, falls below the mean ambient density (Antonini 2013). Following Gnedin et al. (2014), we adopt the average density at the half-mass radius

$$\rho_{\rm h} = 10^3 \frac{M_\odot}{\rm pc^3} \min\left\{10^2, \max\left[1, \left(\frac{M}{2\times 10^5\ M_\odot}\right)^2\right]\right\}. \quad (7)$$

This equation limits $\rho_{\rm h}$ to $10^5\ M_\odot\ {\rm pc}^{-3}$ in the most massive clusters, that is, about the highest observed half-mass density. A cluster is considered disrupted if the average density at the half-mass radius is smaller than the mean ambient density

$$\rho_{\rm h} < \rho_*(r) = \frac{V_{\rm c}^2(r)}{2\pi G r^2} \quad (8)$$

due to the adopted field stellar mass, as well as the growing mass of the nuclear stellar cluster. As the nuclear cluster begins to build up, its stellar density will exceed even the high density of infalling GCs, and these clusters will be directly disrupted before reaching the galaxy center (Gnedin et al. 2014).

We consider the cluster moving on a circular trajectory of radius r and set this radius to be the time-averaged radius of the true, likely eccentric, cluster orbit (Gnedin et al. 2014). We consider the effect of dynamical friction on cluster orbits by evolving the radius r of the orbit according to (Binney & Tremaine 2008)

$$\frac{dr^2}{dt} = -\frac{r^2}{t_{\rm df}}, \quad (9)$$

where

$$t_{\rm df}(r, M) \approx 0.45\left(\frac{M}{10^5\ M_\odot}\right)^{-1}\left(\frac{r}{\rm kpc}\right)^2\left(\frac{V_{\rm c}(r)}{\rm km\ s^{-1}}\right)\ {\rm Gyr}. \quad (10)$$

Several authors have shown the importance of the details of the cluster orbit and its relation with the local tidal field (Tiongco et al. 2016; Madrid et al. 2017). Webb et al. (2014) showed that eccentric orbits increase the mass-loss rate and cluster velocity dispersion and shorten the GC relaxation time. Since the initial distribution of GC eccentricities is not well understood, and to keep things simple, we include the effect of the deviation of the GC orbit from circular by including an eccentricity correction factor $f_e = 0.5$ in the dynamical friction equations, consistent with the results of simulations by Jiang et al. (2008).

We describe the Milky Way's potential following Gnedin et al. (2014) with a central black hole ($M_{\rm BH} = 4\times 10^6\ M_\odot$), a Sérsic profile (Sérsic 1963; see also Terzić & Graham 2005) with total mass $M_{\rm S} = 5\times 10^{10}\ M_\odot$ and effective radius $R_{\rm e} = 4$ kpc, and a dark matter halo ($M_{\rm DM} = 10^{12}\ M_\odot$ and $r_{\rm s} = 20$ kpc; Navarro et al. 1997; see also Fragione et al. 2018 and Fragione & Loeb 2017). We continuously update the Galactic mass distribution to include the gaseous and stellar debris from the disrupted GCs as the nuclear star cluster begins to form (Gnedin et al. 2014).

3. IMBH Merger History and Evolution

Because of the short lifetimes of massive stars, they collapse into SBHs soon after cluster formation. Assuming a standard Kroupa (2001) initial mass function, the number of SBHs is roughly proportional to the initial cluster mass (O'Leary et al. 2006),

$$N_{\rm SBH} \approx 3\times 10^{-3}\frac{M_{\rm GC}}{M_\odot}. \quad (11)$$

Due to dynamical friction, the SBHs segregate toward the GC center on timescales

$$t_{\rm seg} \approx \frac{\bar{m}}{M_{\rm SBH}} t_{\rm rh}, \quad (12)$$

where $\bar{m}$ and $M_{\rm SBH}$ are the average stellar mass and SBH mass, respectively, and $t_{\rm rh}$ is the half-mass relaxation time. In a few tens of Myr, the SBHs form a self-gravitating subsystem within the core, dynamically decoupled from the rest of the cluster, until recoupling with the rest of the stars (Spitzer 1969). The dynamical evolution of the SBH subsystem proceeds on a timescale shorter than the cluster dynamical timescale by a factor $\approx N_{\rm BH}/N$. As widely discussed in the literature, these SBHs can undergo strong gravitational interactions with other BHs and are likely ejected from the cluster, causing a progressive depletion of the BH subcluster. If a GC is Spitzer unstable, very high central SBH densities are reached, and the central IMBH can grow due to subsequent mergers with SBHs (Miller & Hamilton 2002). While the Spitzer instability criterion is well satisfied from the beginning of the cluster's evolution, SBHs may recouple to the rest of the cluster at later times as the cluster evolves and loses mass. For instance, for a GC mass of $10^5\ M_\odot$, the Spitzer criterion would require less than ≈30–50 SBHs to be stable, assuming that all of the SBHs

are 10 $M_\odot$. The SBH mass function would even reduce this number (O'Leary et al. 2006). Recently, Morscher et al. (2013, 2015) used more realistic Monte Carlo simulations of GCs with a BH mass spectrum. Their results showed that many of the old massive GCs could still retain tens of SBHs up to the present day, making such clusters still Spitzer unstable (see also Breen & Heggie 2013; Arca-Sedda 2016).

In case the center of the cluster hosts an IMBH, one of the SBHs forms a bound pair with the central IMBH. Leigh et al. (2014) showed that such an event takes $\lesssim$100 Myr of cluster evolution. Then, the remaining SBHs undergo strong interactions with the central SBH-IMBH binary, which may merge and be ejected out of the cluster because of GW recoil kick. If not, the IMBH merger remnant will capture another SBH on a timescale comparable to the timescale of SBH ejection (Leigh et al. 2014). Typically, the second SBH companion is lighter than the first one and $T_{\rm GW}$ becomes longer, decreasing the rate of IMBH-SBH mergers. Gültekin et al. (2004) found that the IMBH-SBH binary continuously interacts with objects in the cluster and will have a very high eccentricity after its last encounter before inspiraling and merging due to GWs, with a large fraction retaining a measurable eccentricity ($0.1 \lesssim e \lesssim 0.2$). O'Leary et al. (2006) found that the typical merger rate is made up of two phases: the first when the cluster is undergoing a lot of binary interactions and the second when the binary fraction is depleted and nearly zero, which scales roughly as t^{-1}. The typical timescale for the central dark subcluster to deplete all the SBHs may range from a few 100 Myr to several Gyr depending on the cluster mass, more massive being longer. Actually, the timescale for all BHs to be ejected increases with larger cluster mass, both because the initial number of SBHs is larger and because the relaxation time is longer (Leigh et al. 2014). In the meantime, the host GC loses mass and shrinks its orbit as a consequence of dynamical friction (Section 2).

During the first moments of its lifetime, the binary SBH-IMBH usually has very high eccentricities and typically decreases its semimajor axis due to dynamical friction and later to scattering slingshots with ambient objects at the typical hardening radius (Milosavljević & Merritt 2001; Merritt 2013)

$$a_{\rm h} = \frac{M_{\rm SBH}}{M_{\rm IMBH}+M_{\rm SBH}}\frac{r_{\rm inf}}{4}, \tag{13}$$

where $r_{\rm inf} = GM_{\rm IMBH}/\sigma_{\rm c}^2$ is the influence radius of the IMBH, $\sigma_{\rm c}$ is the cluster central velocity dispersion, $M_{\rm IMBH}$ and $M_{\rm SBH}$ are the masses of the IMBH and SBH, respectively, and $a_{\rm h}$ ranges from a few au in the most massive clusters to a few 100 au in the lightest ones, which have smaller velocity dispersions and less massive IMBHs. The binary is hardened by three- and four-body interactions and may form stable hierarchical triples where the Kozai–Lidov resonances become important (Kozai 1962; Lidov 1962) on a typical timescale

$$T_{\rm LK} \approx \frac{P}{2\pi}\frac{M_{\rm IMBH}+M_{\rm SBH}}{M_{\rm SBH,out}}\left(\frac{a_{\rm out}}{a_{\rm in}}\right)^3(1-e_{\rm out}^2)^{3/2}. \tag{14}$$

Here P is the period of the IMBH-SBH binary, $M_{\rm SBH,out}$ is the mass of the external companion, $a_{\rm in}$ is the IMBH-SBH semimajor axis, and $a_{\rm out}$ and $e_{\rm out}$ are the semimajor axis and eccentricity of the outer orbit, respectively. High eccentricities are fundamental to making the binary enter the GW regime even at high semimajor axis, and the Kozai–Lidov oscillations may play an important role in increasing the eccentricity of the IMBH-SBH binary. Three-body interactions may lead to the ejection of the binary if its semimajor axis is below (Antonini & Rasio 2016)

$$a_{\rm ej} = \frac{0.2G\mu M_{\rm SBH,out}^2}{(M_{\rm IMBH}+M_{\rm SBH})(M_{\rm IMBH}+M_{\rm SBH}+M_{\rm SBH,out})v_{\rm esc}^2}, \tag{15}$$

where μ is the binary reduced mass. As the IMBH-SBH binary hardens, the typical time to the next interaction falls below the GW timescale, when the semimajor axis of the binary becomes smaller than (Haster et al. 2016)

$$a_{\rm GW} \approx \frac{0.06\ {\rm au}}{(1-e^2)^{7/10}}\left(\frac{M_{\rm IMBH}}{10^2\ M_\odot}\right)^{1/5}\left(\frac{10^5\ {\rm pc}^{-3}}{n_{\rm c}}\right)^{1/5}, \tag{16}$$

where e is the eccentricity of the IMBH-SBH binary and $n_{\rm c}$ is the number density of stars and BHs in the cluster center. If $a_{\rm GW} > a_{\rm ej}$, the merger occurs before the binary is ejected via three-body interactions. At this point, the semimajor axis and eccentricity of the IMBH-BH binary evolve according to (Peters 1964)

$$\frac{da}{dt} = -\frac{64}{5}\frac{G^3M_{\rm IMBH}M_{\rm SBH}M}{c^5a^3(1-e^2)^{7/2}}\left(1+\frac{73}{24}e^2+\frac{37}{96}e^4\right), \tag{17}$$

$$\frac{de}{dt} = -\frac{304}{15}\frac{G^3M_{\rm IMBH}M_{\rm SBH}M}{c^5a^4(1-e^2)^{5/2}}\left(e+\frac{121}{304}e^3\right), \tag{18}$$

and the binary merges within

$$T_{\rm GW} = \frac{3}{85}\frac{a^4c^5}{G^3M_{\rm IMBH}M_{\rm SBH}M}(1-e^2)^{7/2}, \tag{19}$$

where $M = M_{\rm IMBH}+M_{\rm SBH}$. Leigh et al. (2014) illustrated that in N-body simulations, $T_{\rm GW}$ may even be of the order of 1 Myr or less because of the very high eccentricities reached by the IMBH-BH binary.

As shown by N-body simulations (Konstantinidis et al. 2013; Haster et al. 2016), the merging of the binary IMBH-SBH happens after a few Myr. When merging occurs, the merger remnant undergoes a recoil kick and acquires a velocity (Lousto et al. 2012)

$$\boldsymbol{v}_{\rm kick} = (1+e)[v_m\hat{\boldsymbol{e}}_{\perp,1} + v_\perp(\cos\xi\hat{\boldsymbol{e}}_{\perp,1} + \sin\xi\hat{\boldsymbol{e}}_{\perp,2}) + v_\parallel\hat{\boldsymbol{e}}_\parallel], \tag{20}$$

where

$$v_m = A\eta^2\sqrt{1-4\eta}(1+B\eta), \tag{21}$$

$$v_\perp = \frac{H\eta^2}{1+q}(\chi_{2,\parallel} - q\chi_{1,\parallel}), \tag{22}$$

and

$$v_\parallel = \frac{16\eta^2}{1+q}[V_{1,1} + V_A\tilde{S}_\parallel + V_B\tilde{S}_\parallel^2 + V_C\tilde{S}_\parallel^3] \times |\boldsymbol{\chi}_{2,\perp} - q\boldsymbol{\chi}_{1,\perp}|\cos(\phi_\Delta - \phi_1). \tag{23}$$

In Equation (20), we included a term $(1+e)$ to take into account the eccentricity contribution for eccentric orbits, since IMBH-SBH binaries may not have completely circularized by

the time of the merger (Sopuerta et al. 2007; Holley-Bockelmann et al. 2008). In the previous equations, $\eta = q/(1+q)^2$ is the symmetric mass ratio. The symbols $\perp$ and $\parallel$ refer to the direction perpendicular and parallel to the orbital angular momentum, respectively, while $\hat{e}_\perp$ and $\hat{e}_\parallel$ are orthogonal unit vectors in the orbital plane. Moreover,

$$\tilde{\boldsymbol{S}} = 2\frac{\boldsymbol{\chi}_{2,\perp} + q^2\boldsymbol{\chi}_{1,\perp}}{(1+q)^2}, \tag{24}$$

$A = 1.2 \times 10^4\,\mathrm{km\,s^{-1}}$, $H = 6.9 \times 10^3\,\mathrm{km\,s^{-1}}$, $B = -0.93$, $\xi = 145°$ (González et al. 2007; Lousto & Zlochower 2008), and $V_{1,1} = 3678$, $V_A = 2481$, $V_B = 1793$, $V_C = 1507\,\mathrm{km\,s^{-1}}$ (Lousto et al. 2012). Finally, ϕ_1 is the phase angle of the binary and ϕ_Δ is that between the in-plane component of the vector $\Delta_\perp$ of the vector

$$\boldsymbol{\Delta} = M^2\frac{\boldsymbol{\chi}_2 - q\boldsymbol{\chi}_1}{1+q}. \tag{25}$$

During a merger, GWs radiate not only linear momentum but also angular momentum and energy. In our calculations, we adjust the total spin and mass of the merger remnant to account for these losses (Lousto et al. 2010). This allows us to follow the remnant IMBH spin and mass self-consistently.

4. Numerical Setup

We evolve the primordial GC population by means of the equations described in Section 2 according to the prescriptions in Gnedin et al. (2014). We assume that clusters formed at redshift $z = 3$ and calculate their evolution for 11.5 Gyr until today or their eventual tidal disruption or evaporation. Different models predict different initial seeds for the IMBH (Holley-Bockelmann et al. 2008). Portegies Zwart (2006) showed via N-body simulations that runaway collisions in a dense stellar cluster give a typical mass

$$M_{\rm IMBH} \approx m_{\rm s} + 4 \times 10^{-3} f_{\rm c}\,\ln\Lambda\,M_{\rm GC}, \tag{26}$$

where $m_{\rm s} = 50\ M_\odot$ is the mass of the seed-heavy star that initiates the runaway mergers, $\ln\Lambda = 10$ is the Coulomb logarithm, and $f_{\rm c} = 0.2$ is a runaway efficiency factor. The previous equation gives an IMBH with ≈1% of the mass of the cluster. Sesana et al. (2012) proposed to derive the IMBH masses with a low-mass extrapolation of the M–σ relation observed in galactic bulges (Merritt 2013),

$$M_{\rm IMBH} = 2 \times 10^6 \sigma_{70}^4\ M_\odot, \tag{27}$$

where σ_{70} is the velocity dispersion in units of $70\,\mathrm{km\,s^{-1}}$. This equation typically gives a mass one order of magnitude smaller than Equation (26). IMBHs may also have been generated as a consequence of the collapse of a Pop III star. The IMBH remnant may be as massive as a few hundred solar masses (Madau & Rees 2001) or several thousands of solar masses via extreme accretion flows (Woods et al. 2017). Such a conclusion depends significantly on the mass of the Pop III star progenitor, which should have been thousands of solar masses, and on their initial mass function, both being highly uncertain. Predictions of the IMBH mass in the accretion disk fragmentation scenario are even more uncertain (McKernan et al. 2012, 2014). In our simulations, we considered all the clusters hosting an IMBH at their center from the beginning of the cluster evolution. This conclusion is supported by the fast scenario discussed in Giersz et al. (2015), as well as by Pop III star origin. On the other hand, the gradual and progressive formation and evolution of an IMBH across the cluster lifetime would reduce the predicted rate of IMRIs at high redshift. We simply generate IMBH masses by scaling the total mass of the GC. We choose the fraction of the GC mass in the IMBH as $f = 0.5\%$, 1%, 2%, and 5%, in order to span all the possible regimes predicted by the previous considerations. Since we assume for the cluster mass that $M_{\rm min} = 10^4\ M_\odot$ and $M_{\rm max} = 10^7\ M_\odot$, the minimum and maximum mass of the IMBHs is between 50 and $5 \times 10^5\ M_\odot$. By scaling the mass of the GCs, we implicitly adopt a similar IMBH initial mass function as used for clusters (Equation (2)), i.e., a power law with negative index $\beta = 2$.

For SBHs, we adopt a power-law distribution of masses

$$\frac{dN_{\rm SBH}}{dM_{\rm SBH}} \propto M_{\rm SBH}^{-\zeta}, \quad M_{\rm S,min} < M < M_{\rm S,max}, \tag{28}$$

where $M_{\rm S,min} = 5\ M_\odot$ and $M_{\rm S,max} = 40\ M_\odot$. We study the dependence of our results as a function of the exponent of the power law by taking $\zeta = 1$, 2, 3, and 4 (O'Leary et al. 2016). The recoil velocity depends on the mass ratio q and is maximum for $q \approx 0.4$ (see Equation (20) and Holley-Bockelmann et al. 2008).

The spin of black holes is still uncertain. The spin of an SBH is mainly determined at birth and depends on the mass of the progenitor star, as well as its spin rate and interior structure. The spin impacts both the recoil velocity and the gravitational radiation waveforms, in particular if the spins are misaligned with the orbital axis (Miller & Miller 2015). Recently, Fishbach et al. (2017) showed that for SBHs forming from a hierarchical sequence of mergers, the distribution of spin magnitudes has a peak at $\chi \approx 0.7$. Heavier SBHs that form from massive stars are expected to have low spins (Amaro-Seoane & Chen 2016; Kushnir et al. 2016; Belczynski et al. 2017), but their spins may become high due to dynamical effects (Zaldarriaga et al. 2017). For IMBHs, the situation is even more complicated (Miller & Miller 2015). In our simulations, we consider several values for the initial IMBH and SBH spins $\chi = 0$, 0.2, 0.5, and 0.7 and account for the effect of the spin in the GW recoil velocity. We note that the equations we use to compute the corrections to the spin of the merger product are expected to give reliable results for nonextreme intrinsic spin magnitudes $\lesssim$0.8–0.9. All of the relevant relative orientations between the spins, angular momenta, and orbital plane are generated according to the prescriptions in Lousto et al. (2010).

The eccentricity of the IMBH-SBH binary plays a role in driving the binary toward merger due to GW emission. Simulations show that the binary orbital eccentricity is usually of order of unity soon after the dynamical formation and as a consequence of the repeated interactions with the stellar surroundings (Leigh et al. 2014). However, as the eccentricity increases, GW emission may eventually dominate the evolution of the binary semimajor axis and eccentricity, which leads to the circularization of the IMBH-BH binary on shorter timescales than the average timescale between encounters with the stellar surroundings (Konstantinidis et al. 2013; Leigh et al. 2014). Gültekin et al. (2006) and O'Leary et al. (2006) showed that the binaries could merge with high eccentricity for GWs detected by *LISA*, while the binary will have circularized by the time GWs are detected by LIGO. Equation (20) depends

on the eccentricity through the factor $(1 + e)$, which is valid only for small eccentricities (Holley-Bockelmann et al. 2008). The exact form of the kick velocity when e approaches high values is not well known, but in general, $v_{\rm kick}$ becomes larger with larger eccentricities. In our fiducial models, we consider circular orbits. Additionally, we run a simulation where all binaries have $e = 0.2$, which makes the recoil velocity 1.2 times larger, according to Equation (20).

The other two parameters to specify are the average number of IMBH-SBH collisions $N_{\rm coll}$ and the average time $t_{\rm coll}$ between subsequent collisions. Holley-Bockelmann et al. (2008) used $N_{\rm coll} = 25$, derived from simulations of Gültekin et al. (2006), assuming that the IMBH-SBH merging phase takes place in the first moments of a GC lifetime. Moreover, Holley-Bockelmann et al. (2008) found that their results were quite insensitive to $N_{\rm coll}$. We note that $N_{\rm coll}$ represents the maximum number of collisions that an IMBH can undergo in a GC. If the IMBH is ejected as a consequence of GW recoil velocity or the host GC dissolves due to Galactic tidal disruption, the number of mergers in that GC will be smaller than $N_{\rm coll}$. It is hard to define $t_{\rm coll}$ and find an analytical expression for all of the cluster mass. As reference, O'Leary et al. (2006) found that the typical merger rate may be described by two phases: the first when the cluster is undergoing a lot of binary interactions and the second when the binary fraction is depleted and nearly zero, which scales roughly as t^{-1}. Leigh et al. (2014) found that this typical timescale for the central dark subcluster to deplete all of the SBHs ranges from a few 100 Myr to several Gyr, depending on the cluster mass. Konstantinidis et al. (2013) evolved a $2 \times 10^4\ M_\odot$ GC with a central 500 $M_\odot$ IMBH and found that the first merger happens ≈50 Myr after the beginning of the simulations. Haster et al. (2016) found a merging event after ≈110 Myr in N-body simulations of a 100 $M_\odot$ IMBH embedded in a cluster with 32 10 $M_\odot$ BHs and 32,000 1 $M_\odot$ stars. To find a simple value of $t_{\rm coll}$ for all of the clusters is not straightforward. We note that $t_{\rm coll}$ may be quantified based on N-body simulations calibrated to IMBH-SBH binaries embedded in a star cluster (Sigurdsson & Phinney 1993; Leigh & Sills 2011). To keep things simple, we adopt $t_{\rm coll} = 50$ Myr in our fiducial model and run additional models with $t_{\rm coll} = 100$, 150, and 200 Myr to study the dependence of the results on this uncertain parameter, in agreement with estimates by Miller (2002). Moreover, we set the maximum number of IMBH-SBH merger events to $N_{\rm coll} = T_{\rm life}/t_{\rm coll}$, where $T_{\rm life}$ is the maximum lifetime of GCs. In our simulations, we assume that all of the clusters formed at $z = 3$, which corresponds to $T_{\rm life} = 11.5$ Gyr.

In our simulations, we only consider the formation and evolution via GW emission of IMBH-BH binaries embedded in the innermost BH subcluster. Moreover, we do not track the dynamical encounters of the IMBH-SBH binary with other SBHs that may kick the binaries out of the host GC and simply assume that each of them merges at fixed time intervals due to the combined effect of these interactions and GWs, independently of their mass. Finally, we note that the IMBH-BH binary may be kicked out by a three-body interaction event, as discussed in the previous section. Equation (15) shows the typical binary semimajor axis below which a three-body interaction will cause the binary to be ejected from the GC. As also discussed in Holley-Bockelmann et al. (2008), a simple estimate of the relative importance of the dynamical kicks and GW recoil kicks is not easy and depends on the details of the interaction, hence on the ambient cluster. However, dynamical kicks may be important (under some circumstances) only for low-mass IMBHs. For instance, Gültekin et al. (2006) found that a 100 $M_\odot$ IMBH is ejected ≈50% of the time if its companion and the third BH are 10 $M_\odot$. In our calculations, we neglect the dynamical kicks for simplicity. However, we note that they would affect low-mass clusters that host low-mass IMBHs, which are very likely to be ejected soon after cluster formation because of GW recoil kicks.

5. Results

We evolve the primordial GC population by means of the equations described in Section 2, according to the prescriptions in Gnedin et al. (2014). While the cluster evolves in the Galactic field, we generate IMBH-SBH merger events once during every $t_{\rm coll}$ time interval. Following each merger, we calculate the recoil velocity using the equations shown in Section 3 and update the total spin and mass of the merger remnant to account for radiation of angular momentum and energy (Lousto et al. 2010, 2012). We compute the escape velocity from the center of a GC,

$$v_{\rm e}(t) = \sqrt{\frac{GM_{\rm GC}(t)}{r_{\rm h}(t)}}, \tag{29}$$

where $r_{\rm h}(t)$ is the half-mass radius at time t, computed using Equation (7). As also discussed in Section 2, Webb et al. (2014) showed that eccentric orbits may affect the overall properties of GCs, such as their half-mass radius. This would in turn affect the expected cluster escape speed. However, since we do not know the initial eccentricity distribution of GCs and how the cluster eccentricity affects the half-mass radius of GCs as function of time and cluster mass, we simply adopt the eccentricity parameter f_e of Gnedin et al. (2014) to crudely account for eccentricity effects and use the half-mass radius as computed from Equation (7). If $|\boldsymbol{v}_{\rm kick}| > v_{\rm e}(t)$, we assume that the IMBH escaped from the star cluster. If the IMBH does not escape, we continue to evolve the cluster mass and position self-consistently according to the equations in Section 2 and generate a new IMBH-SBH merger after $\delta t = t_{\rm coll}$. If $|\boldsymbol{v}_{\rm kick}| < v_{\rm e}(t)$ after $N_{\rm coll}$ merger events, and the IMBH is not ejected from the star cluster, two outcomes are viable. First, the cluster may be dissolved by the Galactic tidal field. We define the IMBH in this channel to have a dissolved GC host. Second, the GC survives and the IMBH remains in the cluster core. To summarize, there are three possible outcomes for each IMBH in a GC:

1. the IMBH is ejected from the star cluster as a consequence of the recoil velocity kick;
2. the IMBH is not ejected due to collisions, but the cluster is dissolved by evaporation and/or tidal disruption in the galaxy; and
3. the IMBH is retained in the cluster, and the cluster remains intact until present.

As discussed in the previous section, several parameters play a role in the fate of the central IMBH. To check the effect of each of them, we run five different models. Table 1 summarizes all the models considered in this work. Every result is the average over $\mathcal{N} = 1000$ realizations.

Table 1
Models: Name, Initial Fraction of Cluster Mass in IMBH (f), Spin (χ), Slope of the SBH Mass Distribution (ζ), Eccentricity (e), Number of Collisions ($N_{\rm coll}$), Time between Collisions ($t_{\rm coll}$), Number of Realizations ($\mathcal{N}$)

Name	f (%)	χ	ζ	e	$t_{\rm coll}$ (Myr)	$\mathcal{N}$
Model 1	0.5–4	0	1	0	50	1000
Model 2	1	0	1–4	0	50	1000
Model 3	1	0–0.7	1	0	50	1000
Model 4	1	0	1	0–0.2	50	1000
Model 5	1	0	1	0	50–200	1000

5.1. IMBH Mass Distribution in Different Channels

In Model 1 (see Table 1), we vary the initial mass of the IMBH relative to the initial mass of the cluster, $f = M_{\rm IMBH}/M_{\rm GC}$, between 0.5% and 4%. Since $M_{\rm GC,min} = 10^4\ M_\odot$ and $M_{\rm GC,max} = 10^7\ M_\odot$, the minimum and maximum mass of the IMBHs are 50 and $5 \times 10^4\ M_\odot$, respectively, in the case of $f = 0.5\%$, while it is 400 and $4 \times 10^5\ M_\odot$, respectively, when $f = 4\%$.

In this model, both the IMBH and the SBHs have no initial spin. The SBH mass is sampled from a distribution $dN/dm = m^{-1}$, i.e., $\zeta = 1$ in Equation (28), and all merger events are assumed to have $e = 0$. In total, we generate at most $N_{\rm coll} = 230$ merger events separated by time intervals of $t_{\rm coll} = 50$ Myr. As noted, $N_{\rm coll}$ represents the maximum number of collisions that an IMBH can undergo. If the IMBH is ejected or the host GC dissolves due to tidal disruption, the number of mergers will be smaller than $N_{\rm coll}$.

Table 2 reports the relative fraction of systems with different outcomes: IMBHs ejected from the GC, IMBHs whose host GC dissolves, and IMBHs that remain within their host GC, which survives until the present. The table also displays the average number of mergers per GC. We find that most of the IMBHs are ejected from the star cluster. IMBHs are retained only in massive GCs, and their relative fraction does not depend on f. Even for $f = 0.5\%$, the IMBHs in these clusters experience very small recoil velocities due to very small mass ratios, and the GCs have very large escape velocities. By increasing f, hence $M_{\rm IMBH}$, the probability of IMBHs being ejected from the cluster by the present decreases, while the fraction of IMBHs with dissolved hosts becomes larger.

Figure 1 shows the resulting distributions for the mass of the IMBH in the three different channels as a function of f. The top panel illustrates the masses of IMBHs that are ejected from their parent clusters as a consequence of the GW merger kicks. The larger the f, the larger the peak mass of the distribution. Even for $f = 4\%$, the mass distribution of ejected IMBHs is peaked at $\lesssim 1000\ M_\odot$. The majority of the IMBHs in this channel come from low-mass clusters. Since the initial GC mass distribution has a negative power law (see Equation (2)), most of the clusters have mass $\lesssim 10^5\ M_\odot$, and, as a consequence, most of the IMBHs have mass $\lesssim 10^3\ M_\odot$. For this population, the recoil velocity is large compared to IMBHs in more massive clusters because of their smaller mass ratios (Equation (20)), and their host GCs have the lowest escape velocities because of their light masses. As a consequence, the IMBHs in this regime are ejected from their parent clusters soon after cluster formation. Finally, we note that such ejected IMBHs may even escape their host galaxy as a consequence of the GW velocity kick. However, in case the BH spin is zero, the kick velocity is typically not large enough to overcome the Galactic potential well, as it is at the maximum of the order of $\approx 200\ {\rm km\ s^{-1}}$ in this case. When the effect of the spin is taken into account, the kick velocity may be as large as a few thousand $\rm km\ s^{-1}$, and IMBHs may escape their host galaxy (see Section 5.4).

Table 2
Branching Ratios of Different Channels and Average Number of Mergers per GC as a Function of the Initial $f = M_{\rm IMBH}/M_{\rm GC}$

f (%)	Ejected (%)	Dissolved (%)	Retained (%)	$\langle N \rangle$
0.5	93.0	4.2	2.8	13.2
1	88.3	8.9	2.8	17.5
2	80.2	17.0	2.8	22.8
4	67.0	30.2	2.8	28.0

The central panel of Figure 1 illustrates the mass of the IMBHs with a dissolved GC host. The distributions are peaked at $\approx$1000–3000 $M_\odot$ and are roughly independent of the GC mass fraction in the IMBH. The IMBHs that belong to this class were born in GCs of intermediate masses. In these GCs, the recoil velocity is smaller than for the ejected IMBHs as a consequence of the smaller q, and the escape velocity from the cluster is larger as a consequence of an initial larger mass. Hence, the IMBHs hosted in such clusters tend to be retained without being ejected after a few collisions. We also note a tail of the $M_{\rm IMBH}$ distribution up to $\approx 10^5\ M_\odot$. These IMBHs were members of the most massive GCs, the ones with masses near $M_{\rm GC,max} = 10^7\ M_\odot$. Due to their short dynamical friction timescales (i.e., a few Gyr for $M_{\rm GC} \gtrsim 10^6\ M_\odot$), such clusters are transported to the galactic center and are tidally disrupted by the Galactic gravitational field (Equation (8)). In our model with $f = 1\%$, we find that $\approx$0.25% of the primordial IMBH population with mass $\gtrsim 10^4\ M_\odot$ was hosted by GCs of mass $\gtrsim 10^6\ M_\odot$ dissolved by the Galactic field.

The bottom panel of Figure 1 shows the mass of IMBHs retained in GCs. The peak of the distribution is at 4000–20,000 $M_\odot$ depending on f, with larger peak $M_{\rm IMBH}$ values corresponding to larger f. The IMBHs in this channel are in the more massive GCs. Such very massive IMBHs can survive for all of the $N_{\rm coll}$ merger events until the present, mainly for two reasons. First, unlike low-mass IMBHs, these heavier IMBHs are imparted very small kick velocities because of the very unequal mass ratios. Second, the escape velocity from the parent cluster core is relatively large because of the large host GC mass. However, as discussed previously, IMBHs from extremely massive GCs are not retained in intact GCs, as those sink efficiently to the centers of the host galaxies and are disrupted by the strong gravitational field therein.

We note that based on the bottom panel, the IMBH candidate of $\approx$40,000 $M_\odot$ detected in ω Cen (Baumgardt 2017) is the most probable, for initial values $M_{\rm IMBH}/M_{\rm GC} \sim 4\%$ and $M_{\rm IMBH}/M_{\rm GC} \lesssim 1\%$ are highly disfavored. However, the $\approx$2200 $M_\odot$ IMBH in 47 Tuc (Kızıltan et al. 2017) is only possible for initial values $M_{\rm IMBH}/M_{\rm GC} \lesssim 0.5\%$.

5.2. Radial Distribution of IMBHs in the Host Galaxy

For the three outcomes (IMBH ejection, GC dissolution, and IMBH retention), we have evaluated the final spatial distribution of IMBHs. For all IMBHs in the first two outcomes, we estimate the final spatial distribution by evolving their orbit by means of dynamical friction (see Equation (9)). As discussed, all ejected IMBHs are retained by the host galaxy if they do not have spin. In such a case, the total number of IMBHs is of the

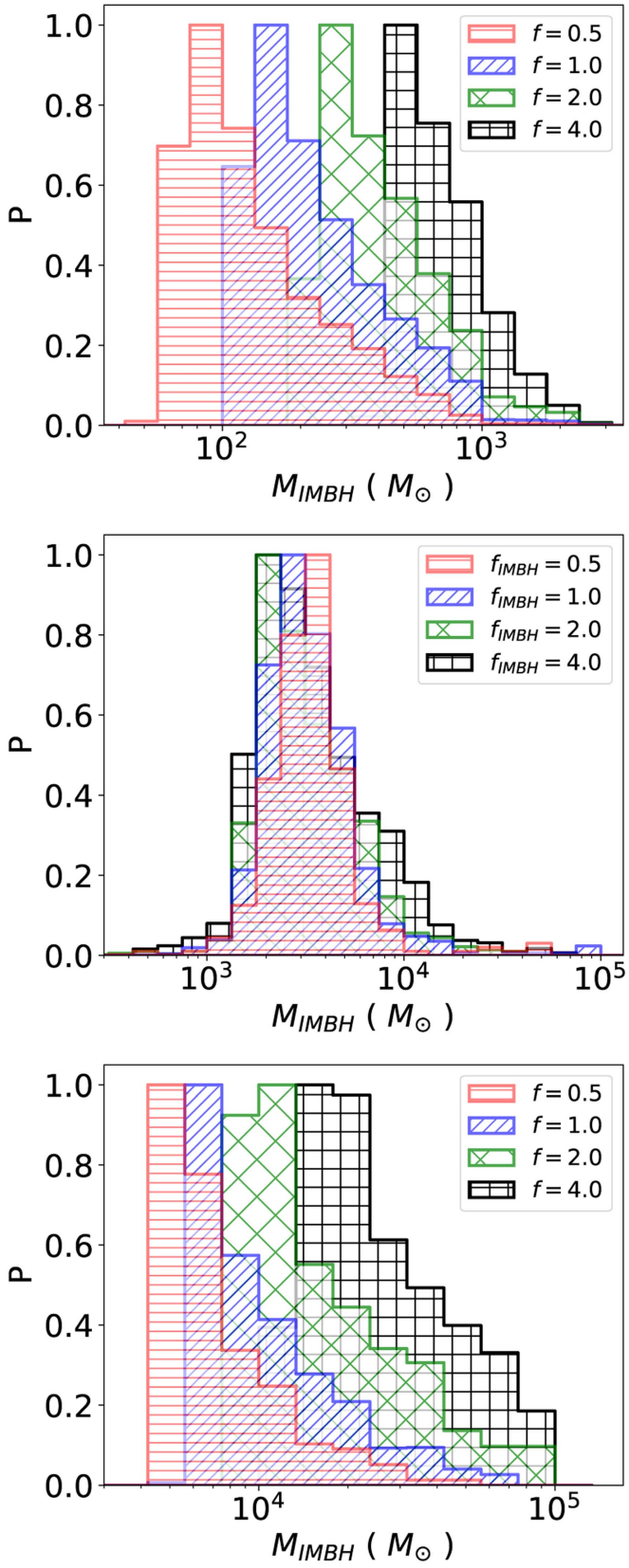

Figure 1. IMBH mass distribution for various initial values $f = M_{\rm IMBH}/M_{\rm GC}$ (shown in the legend in %). The three panels show three different outcomes: IMBHs ejected (top panel), IMBHs with dissolved GC host (center panel), and IMBHs retained (bottom panel). The relative fraction of events for the three different outcomes is shown in Table 2.

order of the primordial population of GCs (≈7000 for the Milky Way). Figure 2 illustrates the spatial distribution and number density of the IMBHs in the three different channels as a function of the radial distance from the galactic center. The IMBHs surviving in clusters map the spatial distribution of the GC population (see Gnedin et al. 2014; Fragione et al. 2018). They are concentrated at ≈10 kpc, where the Galactic tidal field was weak enough to not overcome the self-gravity of their parent clusters. However, IMBHs in the first two channels are peaked at smaller distances (≈5–6 kpc), and their distributions have similar shapes. In the case of IMBHs that are not ejected until the present but are in GCs disrupted by the galaxy, the smaller distances are due to the fact that clusters are more efficiently destroyed where the galaxy's gravitational field is stronger. On the other hand, IMBHs that are ejected as a consequence of the recoil kick velocity are concentrated at small distances, since the primordial GC spatial profile maps the Galactic star distribution and most of the clusters have masses $\lesssim 10^5\ M_\odot$. Figure 3 illustrates the number of IMBHs within a distance R from the galactic center. Our models predict ≈1000 IMBHs within 1 kpc.

5.3. Mass Distribution of IMBH-SBH Mergers

Two of the most interesting quantities that can be measured during a GW event (see Section 6) are the chirp mass ($M_{\rm chirp} = (M_{\rm IMBH}\ M_{\rm SBH})^{3/5}/(M_{\rm IMBH} + M_{\rm SBH})^{1/5}$) and the mass ratio ($q = M_{\rm SBH}/M_{\rm IMBH}$). Figure 4 shows the cumulative distributions Δ of the chirp mass and mass ratio of all of the IMBH-SBH merger events as a function of the initial IMBH mass relative to the GC mass f for Model 1. Small f values imply smaller chirp masses and larger mass ratios. In the case of $f = 0.5\%$, approximately 50% of mergers have chirp mass $\leqslant 120\ M_\odot$, which fraction reduces to 30% for $f = 4\%$. When $f = 0.5\%$, 50% of mergers have $q \lesssim 5 \times 10^{-3}$, while 50% of mergers have $q \lesssim 3 \times 10^{-3}$ if $f = 4\%$. Figure 5 shows the distribution of mass ratios as a function of the chirp mass for different f values. For $f = 0.5\%$, chirp masses of 50 $M_\odot$ may have mass ratios up to ≈0.8, while for $f = 4\%$, the mass ratio is $\lesssim$0.1, independent of the chirp mass of the IMBH-SBH binary.

In Model 2 (see Table 1), we fix the fraction $f = 1\%$ of the initial cluster mass in IMBHs, while SBH masses are sampled from a power-law distribution with negative exponent ζ that we vary between 1 and 4 (Equation (28)). Figure 6 shows the cumulative distribution of the chirp mass and of the Δ of the mass ratio as a function of ζ. Larger ζ implies a smaller number of SBHs with large masses, which imply larger chirp masses. The shallower the slope, the larger the typical chirp mass of the IMBH-SBH merger event. On the other hand, the mass ratio is nearly independent on the slope of the SBH mass distribution.

The slope of the SBH mass distribution ζ also affects the mass of the SBH in the last IMBH-SBH event leading to the ejection due to GW recoil kick. Figure 7 reports the cumulative distribution of the mass of the SBHs responsible for IMBH ejections in the first channel. In the case of $\zeta = 1$, approximately 50% of the SBHs of the last merger have mass $\lesssim 16\ M_\odot$, while 50% of the SBHs of the last merger have mass $\lesssim 4\ M_\odot$ for $\zeta = 4$. Shallower SBH mass functions (smaller ζ) imply a larger number of massive SBHs, hence a larger mass ratio and a higher recoil velocity. As a consequence, the probability of

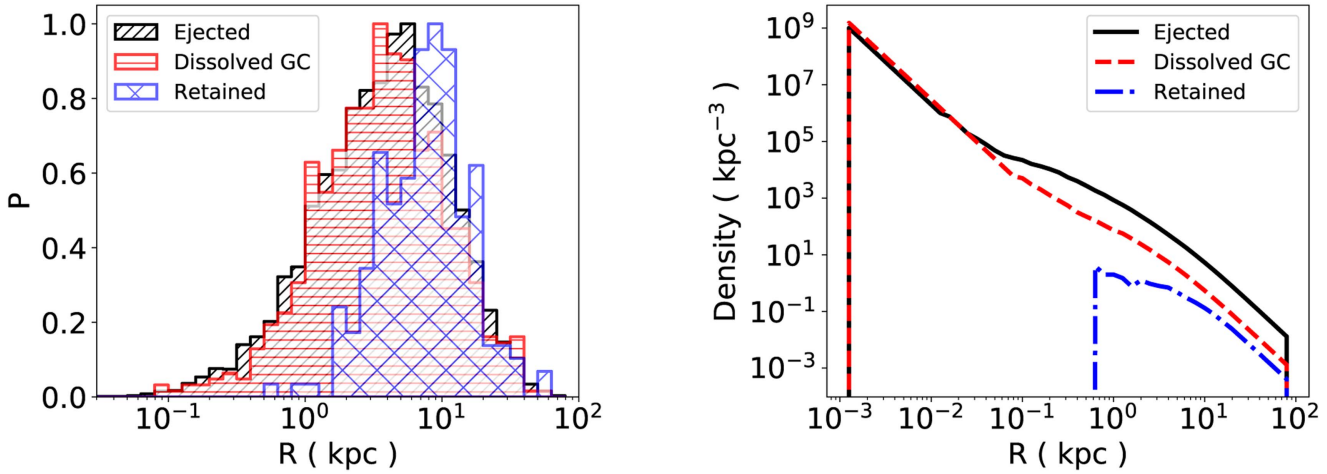

Figure 2. Left panel: final spatial distribution of the IMBHs in the three different channels for Model 1, where the fraction of the GC mass in IMBHs is $f = 1\%$. Right panel: final spatial IMBH number density in the three different channels for Model 1, when the fraction of the GC mass in IMBHs is $f = 1\%$.

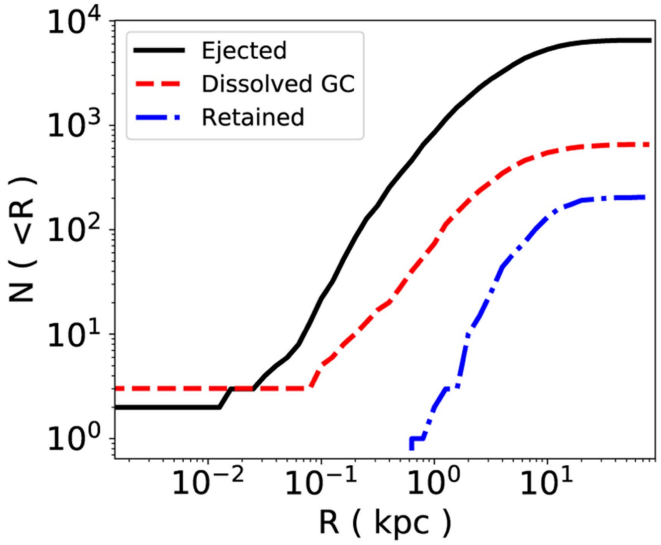

Figure 3. Total number of IMBHs within a distance R from the galactic center in the three different channels for Model 1 when the fraction of the GC mass in IMBHs is $f = 1\%$.

ejected IMBHs when $\zeta = 4$ is smaller by ≈10% than the case of $\zeta = 1$, while the probability of IMBHs in the second channel approximately doubles.

5.4. Spin Effects

In Model 3 (see Table 1), we investigate the role of the spin. In this model, both the IMBH and the SBHs have initial reduced spin χ that we fix to 0.2, 0.5, and 0.7. Different spins are predicted by different physical scenarios. If IMBH mass accumulates by disk accretion, then the spins will be very high, above ≈0.9 (Shapiro 2005); if IMBH mass is created by a large number of mergers, it will be peaked at around 0.7 (Fishbach et al. 2017); and, if it is formed by a collapse of a very massive star, it may be small (Amaro-Seoane & Chen 2016; Belczynski et al. 2017). The spins of the possible IMBHs hosted in the center of a handful of GCs estimated from the observed radio jet luminosity in the Galaxy are in the range 0–0.35 (Buliga et al. 2011).

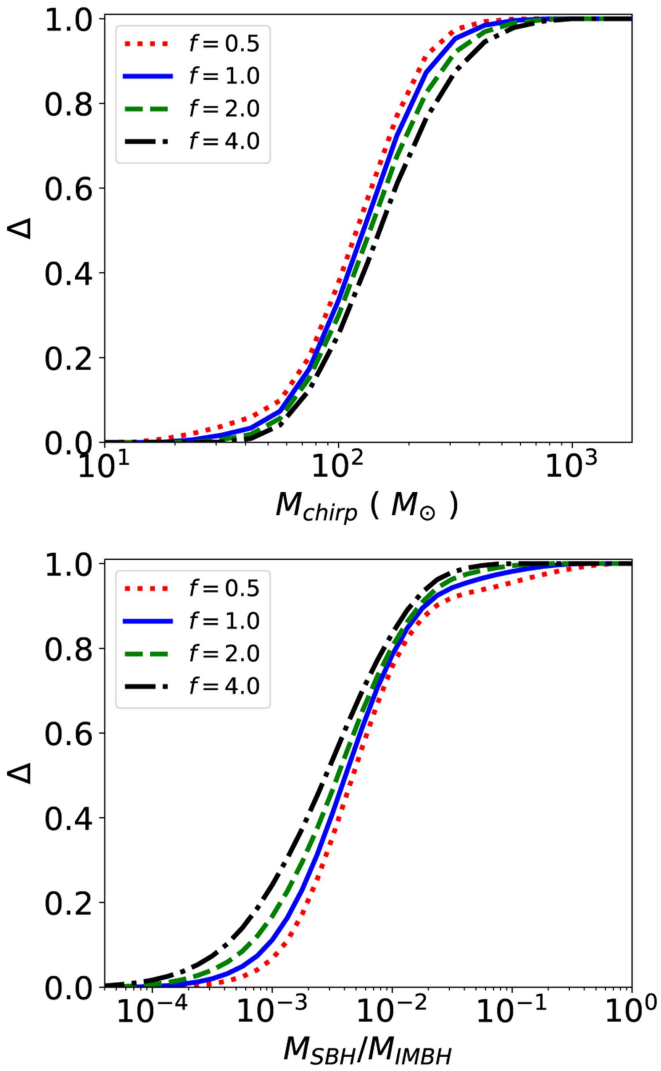

Figure 4. Chirp mass (top) and mass ratio (bottom) cumulative functions of the IMBH-SBH merger events as a function of the fraction f of the cluster mass in IMBHs.

Large spins imply larger recoil velocities. However, the exact outcome depends on the geometry and relative orientation of the IMBH-SBH orbital plane and spin directions. In every merger

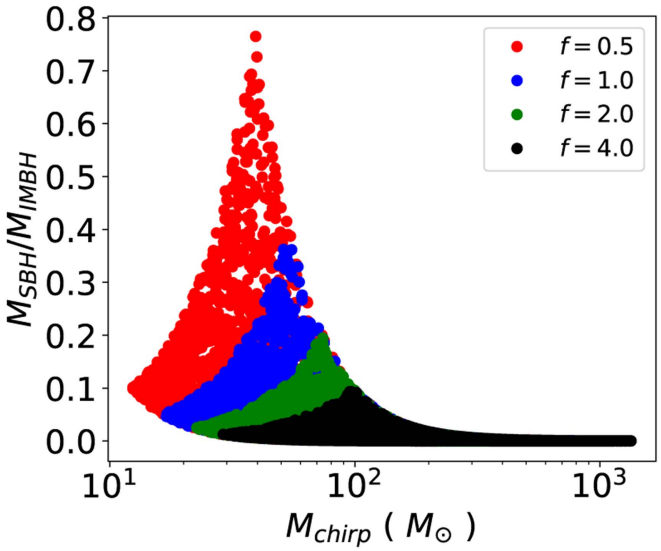

Figure 5. Mass ratio as a function of the IMBH-SBH merger events for different fractions f of the cluster mass in IMBHs.

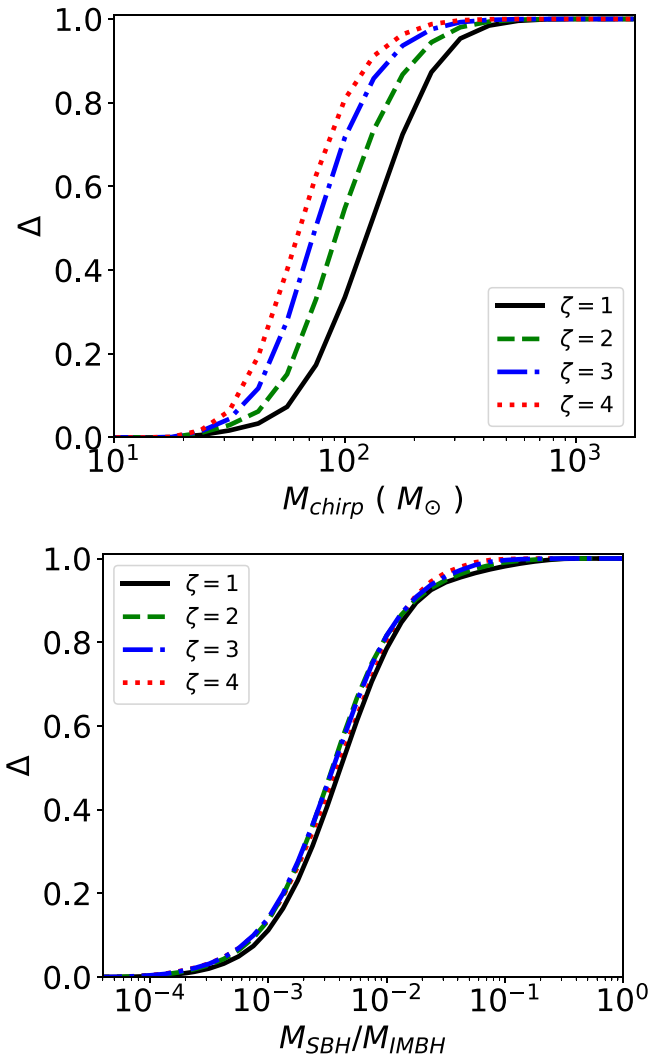

Figure 6. Effect of the slope ζ of the SBH mass function: chirp mass cumulative function (top) and mass ratio cumulative function (bottom).

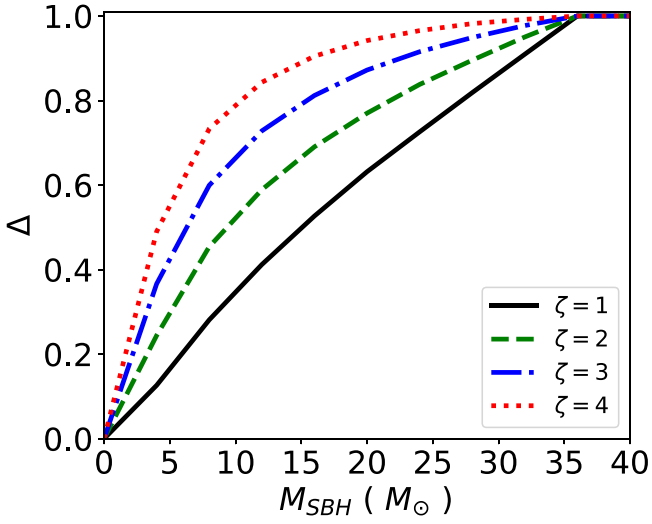

Figure 7. Among clusters in which IMBHs are ejected, the cumulative distribution of the mass of the stellar black hole during the last merger leading to IMBH ejection for various SBH mass function slopes is $-\zeta$.

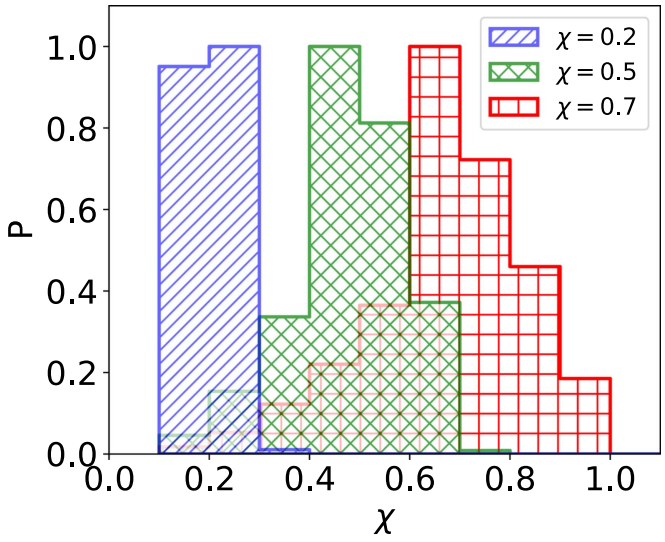

Figure 8. Spin distribution of IMBHs for all merger events as a function of the initial BH spin χ.

event, the spin directions are drawn from an isotropic distribution. All other relevant relative orientations between the spins, angular momenta, and orbital plane are generated according to the prescriptions in Lousto et al. (2010). Figure 8 shows the distribution of spins of the IMBHs for all merger events of Model 3. In this model, both the IMBH and SBH have an initial spin χ. After the merging event, we correct the spin of the merger product to account for these losses (Lousto et al. 2010). After $t_{\rm coll}$, we generate another IMBH-SBH merger, where the IMBH has the spin previously computed and the SBH has spin χ. The resulting distributions of IMRI spins are peaked at nearly the initial χ, with a width that increases with larger values of χ. For equal mass mergers, the final spin is peaked at 0.7, independent of the initial spins, due to the orbital angular momentum of the merging BHs (Hofmann et al. 2016). In general, the final angular momentum parameter χ_f of a merger product is the sum of three

contributions (Buonanno et al. 2008),

$$\chi_f = \frac{L_{\rm orb}(\mu, r_{\rm ISCO}, \chi_f)}{M^3} + \frac{M^3_{\rm IMBH}\chi_{\rm IMBH}}{M^3} + \frac{M^3_{\rm SBH}\chi_{\rm SBH}}{M^3}, \quad (30)$$

where M is the binary total mass; $\chi_{\rm IMBH}$ and $\chi_{\rm SBH}$ are the reduced spins of the IMBH and SBH, respectively; and $L_{\rm orb}(\mu, r_{\rm ISCO}, a_f)$ is the orbital angular momentum of a particle of mass μ at the innermost stable circular orbit (ISCO) of a Kerr black hole of spin parameter χ_f. Being usually $M_{\rm IMBH} \gg M_{\rm SBH}$, the spin of the merger product is dominated by the contribution of the IMBH (with a contribution of the angular momentum). This explains the behavior of the distribution of spins in Figure 8.

As discussed, in Equation (20), the kick velocity is at the maximum of the order of $\approx$200 km s^{-1}. An IMBH can be ejected from the host GC, but its kick velocity may not be large enough to also overcome the Galactic potential well when the BH spin is zero. When the effect of the spin is taken into account, the kick velocity can be as large as a few thousand km s^{-1} (the larger the spin, the larger the recoil velocity), and IMBHs can also escape their host galaxy. Figure 9 shows the GW recoil velocity for different spins of the IMBH and SBHs (Model 3). We find that, while for the model with an initial spin parameter of $\chi = 0.2$, a negligible fraction of IMBHs escapes the host galaxy, $\approx$2% and $\approx$7% of the IMBHs ejected from their host GC are also unbounded with respect to the host galaxy in the models with $\chi = 0.5$ and $\chi = 0.7$, respectively; i.e., $\approx$150 and $\approx$500 IMBHs out of the $\approx$7000 of the initial IMBHs are lost by Milky Way–like galaxies when $\chi = 0.7$. The other parameters, as the fraction of GC mass in the IMBH and the slope of the SBH mass function, do not affect the overall result.

As an example, Figure 10 shows the spin and mass evolution of an IMBH of initial mass $1.4 \times 10^3\ M_\odot$ (hosted by a cluster of initial mass $1.4 \times 10^5\ M_\odot$) for different initial spins. As discussed, larger spins imply larger recoil velocities (see Equation (20)). As a consequence, the total number of collisions for $\chi = 0.2$, 0.5, and 0.7 are 25, 20, and 12, respectively. The spin of the IMBH random walks due to repeated mergers starting from the initial value (see Equation (30)) and stops at its final value when the IMBH is ejected from the cluster or has undergone $N_{\rm coll}$ merger events. For what concerns the mass, IMBHs with initial $\chi = 0.2$ grow to a larger mass, since they undergo a larger number of collisions with respect to the cases with initial $\chi = 0.5$ and $\chi = 0.7$.

5.5. Number and Rate of Mergers and Eccentricity Effects

As discussed, the eccentricity of the IMBH-SBH binary may have an important role, since GW emission may drive the binary toward merger for eccentric systems. Equation (20) also depends on the eccentricity through the correction $(1+e)$, which is valid only for small eccentricities (Holley-Bockelmann et al. 2008), since the exact form of the kick velocity when e approaches high values is not well known. As the eccentricity increases, GW emission may dominate the evolution of the binary semimajor axis and eccentricity over dynamical interactions, which leads to the circularization of the IMBH-BH binary with eccentricities down to $\approx 10^{-4}$ until the merger due to GW emission (Peters 1964; O'Leary et al. 2006, 2009). However, many SBHs may undergo mergers with the central IMBH through exchange with

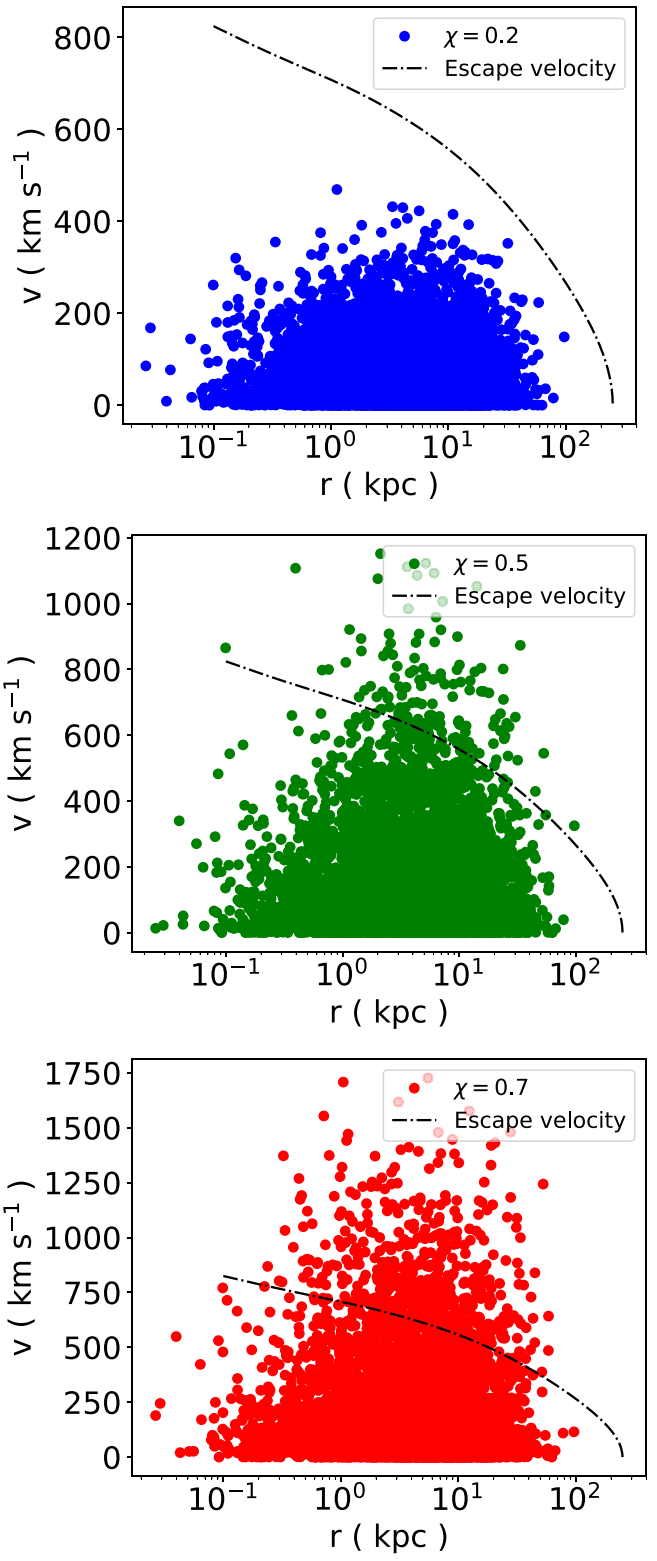

Figure 9. GW recoil velocity for all mergers for different spins of the IMBH and SBH: $\chi = 0.2$ (top), $\chi = 0.5$ (center), and $\chi = 0.7$ (bottom).

lower-mass BHs, and the resulting eccentricity can be high (Miller & Hamilton 2002; Gültekin et al. 2006; Holley-Bockelmann et al. 2008). We run Model 4, in which all the merger events have eccentricity 0.2 and fix the other parameters (see Table 1). According to Equation (20), the kick velocities are 1.2× larger than for circular inspiraling binaries. We find that the eccentricity

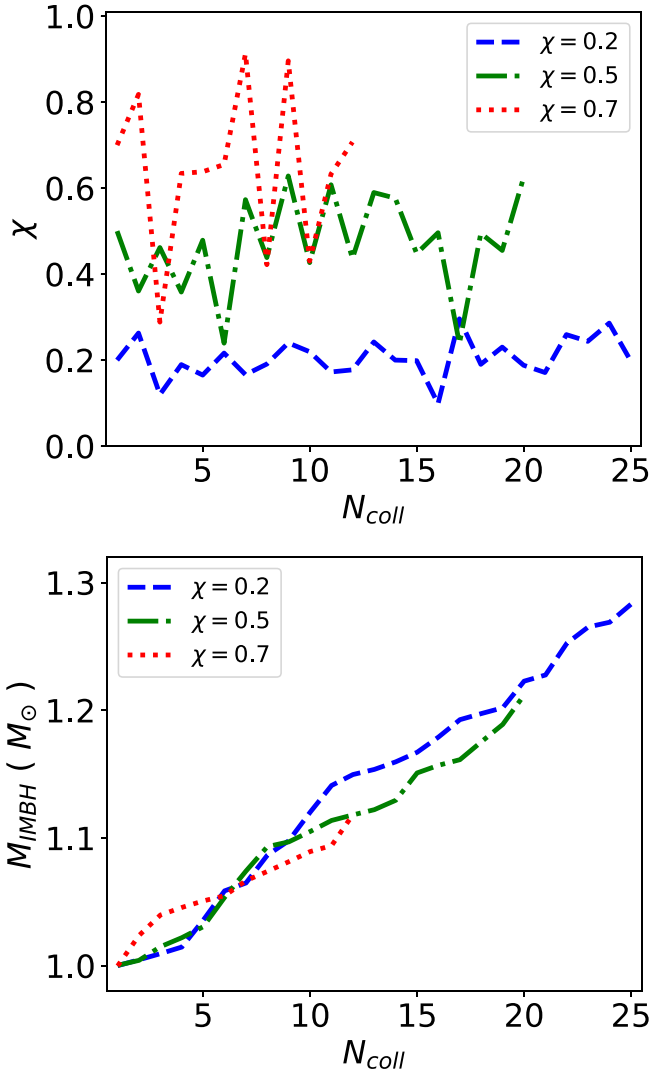

Figure 10. Spin and mass evolution of an IMBH of $1.4 \times 10^3\ M_\odot$ for different initial spins of the IMBH and SBHs.

does not change the overall results presented in the previous sections significantly.

The other two parameters that have to be taken into account are the average number of IMBH-SBH collisions $N_{\rm coll}$ and the average time $t_{\rm coll}$ between two subsequent collisions. For instance, if we assume that $t_{\rm coll} = 50$ Myr, and the binary is made up of 1000 $M_\odot$ IMBHs and 10 $M_\odot$ SBHs orbiting in a circular orbit, the maximum semimajor axis to make the binary merge is $a_{\rm GW} \approx 0.2$ au (see Equation (17)). The typical time to interact with a third body is $\propto a_{\rm GW}^{-1}$ and, in our case, $\approx 10^6$ yr (Antonini & Rasio 2016). Such interactions remove a fraction $\approx 0.2 M_{\rm SBH,3}/M_{\rm IMBH}+M_{\rm SBH}$ of the binary energy ($M_{\rm SBH,3}$ is the mass of the third SBH), making the binary shrink even more. If we require a larger $t_{\rm coll}$, $a_{\rm GW}$ will be larger and the typical time to interact with a third body smaller, making interactions of the IMBH-SBH binary with surrounding BHs more important.

In general, $t_{\rm coll}$ is hard to define, since it may depend on the cluster mass, and the total SBH depletion time may range from a few 100 Myr to several Gyr depending on the cluster mass, as shown by N-body simulations of clusters with a central IMBH by Leigh et al. (2014). Recently, Breen & Heggie (2013) and Morscher et al. (2013, 2015) showed that GCs could retain a lot of BHs until the present day.

In Model 5, we run models with $t_{\rm coll} = 50$, 100, 150, and 200 Myr to study the dependence of the results on this parameter. Such models correspond to a maximum number of IMBH-SBH merger events of $N_{\rm coll} = 230$, 115, 76, and 57, respectively. The main effect of varying $t_{\rm coll}$ is on the inferred rate of IMRI events, as discussed in the next section. In the initial part of the IMBH-SBH merger history, a lot of mergers are due to low-mass GCs, from which the IMBH is ejected as a consequence of the recoil velocity after one or a few merger events. The final part is dominated by mergers with IMBHs in more massive GCs. Only a few of them survive and are not destroyed, and their IMBHs undergo all $N_{\rm coll}$ events. For the others, since the merger events take place later in time for longer $t_{\rm coll}$, their mass is smaller because of tidal stripping by the Galactic field. As a consequence, the GC is disrupted before undergoing $N_{\rm coll}$ merger events or its escape velocity is reduced, and the IMBH may be ejected because of GW recoil velocity. Hence, the total number of merger events is larger for smaller $t_{\rm coll}$, and it is $\approx$30% smaller in the case of $t_{\rm coll} = 200$ Myr with respect to the case of $t_{\rm coll} = 50$ Myr. The other quantities are not significantly affected by the choice of $t_{\rm coll}$.

6. Rate of IMRIs

The study of IMBHs as sources of detectable GWs has been under scrutiny for years (Gültekin et al. 2004; Will 2004; Gültekin et al. 2006; Konstantinidis et al. 2013). In the inspiral phase, the angular-averaged characteristic dimensionless strain amplitude[8] of the GWs emitted by a source at luminosity distance D is (e.g., Kocsis et al. 2011)

$$h_{\rm c} \approx \begin{cases} \frac{4}{5}\frac{G^{5/3}}{c^4}\frac{M_{\rm IMBH}^{5/3} M_{\rm SBH} f_{\rm GW}^{7/6}}{D} T_{\rm obs}^{1/2} & \text{if } f_{\rm GW} \leqslant f_{\rm crit}, \\ \frac{1}{\sqrt{30}\,\pi^{2/3}}\frac{G^{5/6}}{c^{3/2}}\frac{M_{\rm IMBH}^{1/3} M_{\rm SBH}^{1/2}}{D f_{\rm GW}^{1/6}} & \text{if } f_{\rm GW} \geqslant f_{\rm crit}, \end{cases}$$
$$= \begin{cases} 6.2 \times 10^{-22} M_{\rm IMBH,10^3 M_\odot}^{5/3} M_{\rm SBH,10 M_\odot} f_{\rm GW,10\ mHz}^{5/6} \\ \quad \times T_{\rm obs,yr}^{1/2} D_{\rm Gpc}^{-1} \\ \text{if } f_{\rm GW} \leqslant f_{\rm crit}, \\ 1.4 \times 10^{-21} M_{\rm IMBH,10^3 M_\odot}^{1/3} M_{\rm SBH,10 M_\odot}^{1/2} f_{\rm GW,10\ Hz}^{-1/6} D_{\rm Gpc}^{-1} \\ \text{if } f_{\rm GW} \geqslant f_{\rm crit}, \end{cases} \quad (31)$$

where $f_{\rm crit}$ is given by the observation time $T_{\rm obs}$ as

$$f_{\rm crit} = 0.045\ M_{\rm IMBH,10^3 M_\odot}^{-1/4} M_{\rm SBH,10 M_\odot}^{-3/8} T_{\rm obs,yr}^{-3/8}\ {\rm Hz}. \quad (32)$$

To save space, we have introduced a notation for quantities x_a expressed with physical units u as $x_{a,u} \equiv x_a/u$, so that $x_{a,u}$ is dimensionless. For $f_{\rm GW} \lesssim f_{\rm crit}$, the GW frequency emitted by the binary is approximately constant during the observation time $T_{\rm obs}$, and for $f_{\rm GW} \gtrsim f_{\rm crit}$, the binary inspirals during the

[8] That is, the GW strain in a logarithmic frequency bin or, equivalently, the Fourier transform of the time-domain dimensionless GW strain multiplied by the frequency (cf. detector sensitivity; Moore et al. 2015). Angular averaging is over the binary orientation, sky position, and the detector's antenna pattern. If the observation time is much less than the inspiral timescale and the source is circular, the source is approximately monochromatic with frequency $f_{\rm GW} \pm \frac{1}{2} T_{\rm obs}^{-1}$.

observation and spans a frequency range up to the ISCO. *LISA* and aLIGO are expected to be sensitive to GW frequencies between ≈0.1–100 mHz and ≈10–1000 Hz, respectively. As a consequence, the GWs of IMRIs are potentially observable in these frequency ranges. During the inspiral, the GW frequency increases as the IMBH-SBH orbit shrinks until the last stable orbit, which is followed by a rapid coalescence. Because of the quadrupolar nature of GWs, the typical frequency for circular binaries is twice the orbital frequency. At the ISCO,

$$f_{\rm GW,ISCO} = 2f_{\rm orb} \approx 4.4 M^{-1}_{\rm IMBH,10^3 M_\odot} {\rm Hz} \quad (33)$$

for nonspinning IMBHs, and $f_{\rm GW,ISCO}$ is a factor of 15 higher for maximally spinning IMBHs. The GW frequency before the binary reaches the ISCO is smaller than $f_{\rm GW,ISCO}$. After the final inspiral phase, the merger and ringdown phases emit GWs at a higher frequency, where a characteristic ringdown frequency for zero spins is

$$f_{\rm RD} \approx 12 M^{-1}_{\rm IMBH,10^3 M_\odot} {\rm Hz}. \quad (34)$$

and it is a factor of ∼10 higher for nearly maximal spins (Berti et al. 2009). IMRIs involving IMBHs of a few hundred solar masses will first be observable by *LISA* and then by LIGO. On the other hand, IMRIs involving IMBHs more massive than a few thousands solar masses will merge in the *LISA* band and will not be detectable with LIGO.

We now use the results from our simulated GC models to make predictions on the merger rate of IMRIs. The IMRI coalescence rate is still highly uncertain. The main limitation is to consistently model the evolution of GCs, where most of them are thought to take place, by also including GW energy losses. Moreover, clusters lose mass and inspiral toward the center of their galaxy across cosmic time. A conservative estimate of the merger rate of IMRIs formed in GCs is obtained by assuming that GCs in other galaxies have characteristics and histories similar to those in the Milky Way. We compute the merger rate between IMBHs and SBHs per unit volume and time as a function of the redshift z as

$$\mathcal{R}(z) = n_{\rm GC,total}(z)\, \Gamma_{\rm IMRI}(z), \quad (35)$$

where $n_{\rm GC,total}(z) = 0.77\kappa\, [H(z)/H_0]^3\, {\rm Mpc}^{-3}$ is the spatial density of GCs and their remnants, including those that dissolved and those that survived by $z = 0$, $H(z)$ is the Hubble constant at redshift z,[9] and $\Gamma_{\rm IMRI}(z)$ is the redshifted[10] IMRI rate from a single GC that originally formed at redshift $z = 3$. We choose $n_{\rm GC,sur} = 0.77\,{\rm Mpc}^{-3}$ for the local GC density (Rodriguez et al. 2015).[11] Moreover, we correct for $\kappa = N_{\rm GC,in}/N_{\rm GC,sur} = 35$, where $N_{\rm GC,in}$ and $N_{\rm GC,sur}$ are the numbers of primordial GCs and GCs survived till present, respectively (Gnedin et al. 2014), to take into account IMRIs that happened in GCs that have dissolved by $z = 0$. Finally, we compute $\Gamma_{\rm IMRI}$ from the results of our simulations (see Table 2).

LISA may observe an IMBH-SBH binary in the inspiral phase and Advanced LIGO and VIRGO may detect the IMBH-SBH binary in the late inspiral and merger/ringdown phase at a signal-to-noise ratio of 10 to a distance approximately given by[12] (Flanagan & Hughes 1998; Miller 2002; Gair et al. 2011)

$$D_{\rm LIGO,inspiral} = 0.2 \left(\frac{M_{\rm IMBH}}{1000\, M_\odot}\right)^{-1} \left(\frac{M_{\rm SBH}}{10\, M_\odot}\right)^{1/2} {\rm Gpc}, \quad (36)$$

$$D_{\rm LIGO,RD} = 0.6 \left(\frac{M_{\rm IMBH}}{1000\, M_\odot}\right)^{-3/2} \left(\frac{M_{\rm SBH}}{10\, M_\odot}\right) {\rm Gpc}, \quad (37)$$

$$D_{\rm LISA,inspiral} = 0.6 \left(\frac{M_{\rm IMBH}}{1000\, M_\odot}\right)^{1/2} \left(\frac{M_{\rm SBH}}{10\, M_\odot}\right)^{1/2} {\rm Gpc}, \quad (38)$$

$$D_{\rm ET,inspiral} = 3.3 \left(\frac{M_{\rm IMBH}}{1000\, M_\odot}\right)^{1/2} \left(\frac{M_{\rm SBH}}{10\, M_\odot}\right)^{1/2} {\rm Gpc}. \quad (39)$$

The detection range of the VIRGO,[13] KAGRA,[14] and two Advanced LIGO instruments is a factor of 2 larger than that of a single interferometer given above.

Figure 11 shows the IMRI merger rate as a function of the redshift for Model 1 and Model 5 (left panel) from 2 Gyr until present. The right panel shows the merger rates for different IMBH masses for Model 1 for $f = 1\%$. We divide our IMRIs into different mass bins, since different instruments are expected to observe IMRIs with high sensitivity for different IMBH-SBH binary masses, as discussed. The largest rate comes for $10^3\, M_\odot < M_{\rm IMBH} \leqslant 10^4\, M_\odot$, which will be detectable by either *LISA* or ET. Assuming ET will be able to observe GW events with good S/N up to $z \approx 2$ (Amaro-Seoane & Santamaría 2010), our results predict a detection rate of ≈100–300 ${\rm Gpc}^{-3}\,{\rm yr}^{-1}$. Advanced LIGO, VIRGO, and KAGRA will be able to probe the low end ($\lesssim 10^3\, M_\odot$) of the IMBH population up to $z \sim 1.0$. Our models predict a rate of 0.5–20 ${\rm Gpc}^{-3}\,{\rm yr}^{-1}$ for $0.6 \lesssim z \lesssim 1$ for $300\, M_\odot \lesssim M_{\rm IMBH} \lesssim 1000\, M_\odot$. Lighter IMBHs are efficiently ejected by GW recoils or are in clusters dissolved by the galactic tidal field at $z \gtrsim 2.5$. *LISA* may detect IMBHs of all masses, including the population of $\gtrsim 10^4\, M_\odot$ IMBHs that are difficult to detect with even third-generation Earth-based instruments like ET. The corresponding rate density of those massive IMBH-SBH mergers is ≈3–10 ${\rm Gpc}^{-3}\,{\rm yr}^{-1}$ at low redshift, and it is above ≈100 ${\rm Gpc}^{-3}$ for $z \gtrsim 1.5$.

Our conclusions are consistent with the order-of-magnitude estimate of Haster et al. (2016). During their first observing run, LIGO did not detect GWs from IMBHs (Abbott et al. 2016). Recently, Abbott et al. (2017) used such a result to constrain the rate of IMBH mergers with different masses and configurations. They found that for IMBHs of masses between 100 and 300 $M_\odot$ (with spins aligned with the binary orbital angular momentum), the merger rate is constrained to be $\lesssim 0.93\,{\rm Gpc}^{-3}\,{\rm yr}^{-1}$. The predicted merger rate in this mass range in our models is also very low for $z \leqslant 2.5$ (see blue dashed line in Figure 11). However, we emphasize that at design sensitivity, Advanced LIGO/VIRGO/KAGRA may access IMBH masses between 300 and 1000 $M_\odot$, for which our models predict frequent mergers above $z \geqslant 0.6$ (see green dash-dotted line in right panel). These upgraded instruments

[9] To compute $H(z)$, we use $\Omega_m = 0.286$ and $\Omega_\Lambda = 0.714$ for the matter and cosmological constant normalized density, respectively, and $H_0 = 70\ {\rm km\ s^{-1}\ Mpc^{-1}}$ (Planck Collaboration et al. 2016).

[10] We take into account that the observed rate is redshifted by a factor of $1/(1+z)$, where z is the cosmological redshift.

[11] A less conservative estimate by Portegies Zwart & McMillan (2000) predicts $n_{\rm GC} = 2.9\ {\rm Mpc}^{-3}$ for the local GC density.

[12] Here distance refers to luminosity distance, and masses are redshifted masses, which are the source-frame mass times $(1+z)$.

[13] http://www.virgo-gw.eu/

[14] http://gwcenter.icrr.u-tokyo.ac.jp

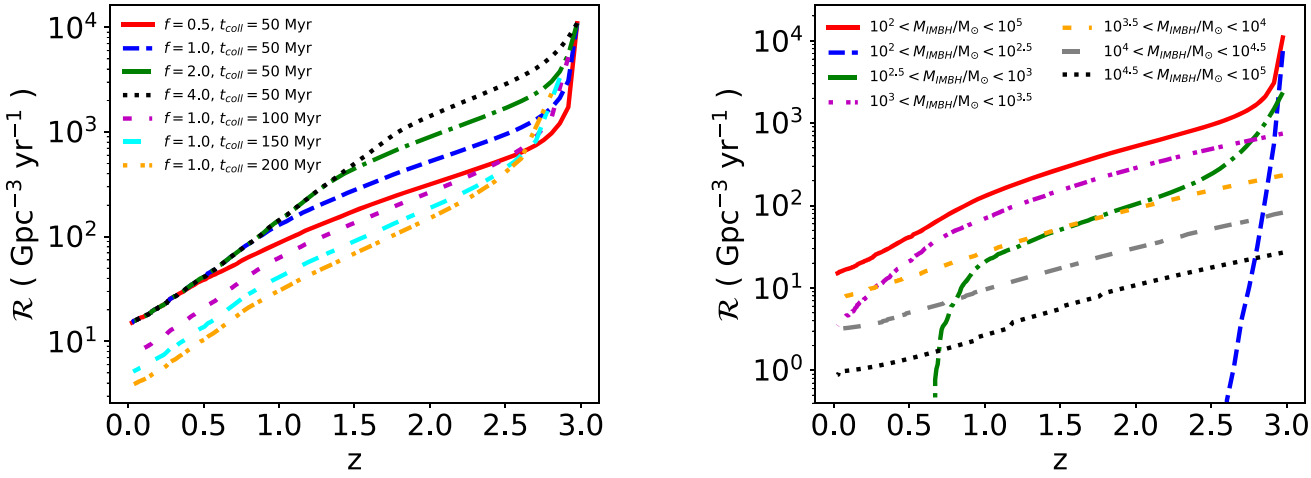

Figure 11. Left panel: rate of IMRIs as a function of redshift for Model 1 and Model 5. Right panel: rate of IMRIs as a function of redshift for different IMBH masses for Model 1, when the fraction of the GC mass in IMBH is $f = 1\%$. Note that LIGO upper limits are currently available only between 100 and 300 $M_\odot$ for z close to zero where the rates are negligible (cf. blue dashed line). However, at design sensitivity, LIGO/VIRGO/KAGRA will measure mergers with masses 300–3000 $M_\odot$ (green and magenta dash-dotted curves), and ET and LISA may access nearly all IMBH mergers shown.

may also detect mergers for rapidly spinning IMBHs between 1000 and 3000 $M_\odot$, where the rates are much higher even at low redshift (see magenta dash-dotted line in right panel).

As discussed in Section 5, the parameters that affect the rate of IMRIs are the fraction of GC mass in the IMBH f, the spin of the BH χ, and the total number of collisions $N_{\rm coll}$. Larger spins imply smaller inferred rates, since the GW recoil kick can be as large as a few thousand km s^{-1}; larger values of f and smaller values of $t_{\rm coll}$ lead to larger rates, since more massive IMBHs suffer from less intense recoil velocities and undergo a larger number of mergers, respectively. By measuring the mass, spin, and redshift distribution of IMBH mergers, GW observations may constrain the GC models.

7. Conclusions

The existence of IMBHs with masses $100\ M_\odot \lesssim M \lesssim 10^5\ M_\odot$ has not yet been confirmed directly. The formation of IMBHs is, however, theoretically very plausible, and one of the formation scenarios requires very dense environments, as in the centers of GCs. The extrapolation of the observed correlation between SMBHs and their stellar environments to this mass range implies that these IMBHs could be present in GCs or dwarf galaxies (Merritt 2013; Baumgardt 2017; Kızıltan et al. 2017). An IMBH would remain dark if not emitting because of accretion but may influence the dynamical evolution of the GC.

GWs will help in the hunt for the first direct evidence of IMBHs. IMBH-SBH binaries may form in GCs and represent so-called IMRIs, a downscaled version of EMRIs. *LISA* will be able to detect tens of IMRIs at any given time (Miller & Hamilton 2002; Amaro-Seoane & Santamaría 2010; Amaro-Seoane et al. 2010). As a consequence of the GW emission, the merger product will be imparted a GW recoil that, according to the mass ratio and spins of the BHs, may be several thousands of km s^{-1} times the square of the symmetric mass ratio (Lousto & Zlochower 2011). Due to the moderate mass ratio of an IMRI and the shallow potential well of a GC, such recoils could be large enough to expel the IMBH from the cluster (Holley-Bockelmann et al. 2008).

In this paper, we have investigated the possibility that primordial GCs were born with a central IMBH, which undergoes merger events with SBHs in the cluster core (Portegies Zwart & McMillan 2000; Leigh et al. 2014; Haster et al. 2016). By means of a semi-analytical method, we have followed the evolution of the primordial cluster population in the galactic potential and the mergers of the binary IMBH-SBH systems (Gnedin et al. 2014; Fragione et al. 2018). We have shown that low-mass IMBHs are usually ejected as a consequence of the GW recoil velocity, while massive IMBHs ($\gtrsim 10^3\ M_\odot$) are left in the Galactic field when their host GC is dissolved. In particular, we predict approximately 10^3 "bare" IMBHs with mass $\gtrsim 10^3\ M_\odot$ each to be left without a host stellar cluster in the inner kpc of the galaxy (Figure 3). The dynamical evolution in the galaxy of this population of IMBHs has been studied by means of dynamical friction, but a more accurate study is needed to determine their final fate and distinguish such a population from the one predicted by cosmological models. Only a small fraction of the IMBHs remain in their host cluster without being ejected due to repeated GW recoil kicks and without the host GC being tidally disrupted by the Galactic field. We have illustrated that the typical chirp mass and mass ratio of an IMRI depend on the initial fraction f of GC mass in IMBHs and also on the slope ζ of the SBH distribution. Larger f and/or shallower slope ζ imply larger typical chirp masses of the IMBH-SBH merger event. We have also investigated the role of the spin in an IMRI. We found that the spin of the final merger product is mostly determined by the initial spin of the IMBH, with a spread due to the geometry of the angular momentum and the spins at the moment of the merging. Moreover, we have shown that larger spins imply larger GW recoil velocity, which leads to $\approx 7\%$ of the primordial IMBHs being ejected from the galaxy. This amounts to a total of ≈ 500 IMBHs ejected per Milky Way–type galaxy and implies an intergalactic IMBH number density of

$$n_{\rm intergalactic\ IMBH} \sim 10\ {\rm Mpc}^{-3}. \quad (40)$$

These estimates are not sensitive to the IMRI eccentricity. However, if the IMBH-SBH collision rate at early times is higher than that in our fiducial model, i.e., $1/(50\ {\rm Myr})$, then the number of IMRI GW events increases.

We have used the average number of IMBH-SBH merger events in our models to predict the rate of IMRIs for current and upcoming GW detections. While IMBHs of any mass can be potentially observed by *LISA*, LIGO is able to spot only

IMBHs with masses of a few hundred $M_\odot$ if it is nonspinning and a few thousand $M_\odot$ if it is maximally spinning. The IMBH-SBH merger rate density decreases in time, from a value of $\mathcal{R} \approx 100\,\mathrm{Gpc^{-3}\,yr^{-1}}$ at $z \gtrsim 2$ to $\mathcal{R} \approx 0.5\,\mathrm{Gpc^{-3}\,yr^{-1}}$ at low redshift (Figure 11). The rate density varies greatly with the IMBH mass, and it is dominated by IMBH masses in the range $10^3\ M_\odot \lesssim M_{\rm IMBH} \lesssim 10^4\ M_\odot$. Current LIGO upper limits exist only for masses $M_{\rm IMBH} \leqslant 300$, where the predicted rate is negligible below $z \lesssim 2.6$. These lighter IMBHs are efficiently ejected by GW recoils or are in clusters dissolved by the galactic tidal field. However, we predict that LIGO/VIRGO/KAGRA may detect IMBH mergers at design sensitivity with $\mathcal{R} \approx 1$–$10\,\mathrm{Gpc^{-3}\,yr^{-1}}$ if it can access the mass range between 300–1000 $M_\odot$ for $z \gtrsim 0.6$ and $\mathcal{R} \approx 5$–$10\,\mathrm{Gpc^{-3}}$ for IMBHs with 1000–3000 $M_\odot$ in the local universe (Figure 11). Assuming *LISA* will be able to observe GW events up to $z \approx 1$ and ET up to $z \approx 2$ (Amaro-Seoane & Santamaría 2010), our results predict a detection rate density of $\approx$100–300 $\mathrm{Gpc^{-3}\,yr^{-1}}$ for IMBHs with a mass of $\approx 10^3$–$10^4\ M_\odot$ with ET and *LISA* and $\approx$3–$10\,\mathrm{Gpc^{-3}\,yr^{-1}}$ for IMBH-SBH binaries with masses $\gtrsim 10^4\ M_\odot$ observable with *LISA*.

We note that the rates at low redshifts may be significantly higher if young massive star clusters host IMBHs. In addition to generating distinct GW events, the large number of inspirals of IMBH-SBH systems at cosmological distances generates an unresolved diffuse GW background (Barack & Cutler 2004), which may affect *LISA* and ET observations.

By measuring the mass, spin, and redshift distribution of IMBH mergers, GW observations may help to improve our understanding of GC and galaxy evolution.

We thank Daniel D'Orazio, Oleg Gnedin, and Deirdre Shoemaker for useful discussions and comments. G.F. acknowledges hospitality from the Eötvös Loránd University of Budapest. This project has received funding from the European Research Council (ERC) under the European Union's Horizon 2020 research and innovation program under grant agreement No. 638435 (GalNUC) and by the Hungarian National Research, Development, and Innovation Office grant NKFIH KH-125675 (to B.K.). This work was performed by BK in part at the Aspen Center for Physics, which is supported by National Science Foundation grant PHY-1607761. I.G. was supported in part by Harvard University and the Institute for Theory and Computation.

ORCID iDs

Giacomo Fragione https://orcid.org/0000-0002-7330-027X
Bence Kocsis https://orcid.org/0000-0002-4865-7517

References

Abbott, B. P., Abbott, R., Abbott, T. D., et al. 2016, ApJL, 818, L22
Abbott, B. P., Abbott, R., Abbott, T. D., et al. 2017, PhRvD, 96, 022001
Abramowicz, M. A., Kluźniak, W., McClintock, J. E., & Remillard, R. A. 2004, ApJL, 609, L63
Amaro-Seoane, P., & Chen, X. 2016, MNRAS, 458, 3075
Amaro-Seoane, P., Eichhorn, C., Porter, E. K., & Spurzem, R. 2010, MNRAS, 401, 2268
Amaro-Seoane, P., Gair, J. R., Freitag, M., et al. 2007, CQGra, 24, R113
Amaro-Seoane, P., & Santamaría, L. 2010, ApJ, 722, 1197
Antonini, F. 2013, ApJ, 763, 62
Antonini, F., & Rasio, F. A. 2016, ApJ, 831, 187
Arca-Sedda, M. 2016, MNRAS, 455, 35
Barack, L., & Cutler, C. 2004, PhRvD, 70, 122002
Baumgardt, H. 2017, MNRAS, 464, 2174
Belczynski, K., Klencki, J., Meynet, G., et al. 2017, arXiv:1706.07053
Berti, E., Cardoso, V., & Starinets, A. O. 2009, CQGra, 26, 163001
Binney, J., & Tremaine, S. 2008, Galactic Dynamics (2nd ed.; Princeton, NJ: Princeton Univ. Press)
Breen, F. G., & Heggie, D. C. 2013, MNRAS, 432, 2779
Buliga, S. D., Globina, V. I., Gnedin, Y. N., et al. 2011, Ap, 54, 548
Buonanno, A., Kidder, L. E., & Lehner, L. 2008, PhRvD, 77, 026004
Capuzzo-Dolcetta, R., & Fragione, G. 2015, MNRAS, 454, 2677
Chernoff, D. F., & Weinberg, M. D. 1990, ApJ, 351, 121
Davis, S. W., Narayan, R., Zhu, Y., et al. 2011, ApJ, 734, 111
Fabbiano, G. 2006, ARA&A, 44, 323
Fishbach, M., Holz, D. E., & Farr, B. 2017, ApJL, 840, L24
Fragione, G., Antonini, F., & Gnedin, O. Y. 2018, MNRAS, 475, 5313
Fragione, G., & Capuzzo-Dolcetta, R. 2016, MNRAS, 458, 2596
Fragione, G., Capuzzo-Dolcetta, R., & Kroupa, P. 2017, MNRAS, 467, 451
Fragione, G., & Ginsburg, I. 2017, MNRAS, 466, 1805
Fragione, G., & Gualandris, A. 2018, MNRAS, 475, 4986
Fragione, G., & Loeb, A. 2017, NewA, 55, 32
Fragione, G., & Sari, R. 2018, ApJ, 852, 51
Freitag, M., Gürkan, M. A., & Rasio, F. A. 2006, MNRAS, 368, 141
Gair, J. R., Mandel, I., Miller, M. C., & Volonteri, M. 2011, GReGr, 43, 485
Gieles, M., & Baumgardt, H. 2008, MNRAS, 389, L28
Gieles, M., Heggie, D. C., & Zhao, H. 2011, MNRAS, 413, 2509
Giersz, M., Leigh, N. W., Hypki, A., Lützgendorf, N., & Askar, A. 2015, MNRAS, 454, 3150
Gnedin, O. Y., Ostriker, J. P., & Tremaine, S. 2014, ApJ, 785, 71
González, J. A., Sperhake, U., Brügmann, B., Hannam, M., & Husa, S. 2007, PhRvL, 98, 091101
Gualandris, A., Gillessen, S., & Merritt, D. 2010, MNRAS, 409, 1146
Gualandris, A., & Merritt, D. 2009, ApJ, 705, 361
Gültekin, K., Miller, M. C., & Hamilton, D. P. 2004, ApJ, 616, 221
Gültekin, K., Miller, M. C., & Hamilton, D. P. 2006, ApJ, 640, 156
Haster, C.-J., Antonini, F., Kalogera, V., & Mandel, I. 2016, ApJ, 832, 192
Hofmann, F., Barausse, E., & Rezzolla, L. 2016, ApJL, 625, L19
Holley-Bockelmann, K., Gültekin, K., Shoemaker, D., & Yunes, N. 2008, ApJ, 686, 829
Hopman, C., & Alexander, T. 2006, ApJL, 645, L133
Flanagan, É. É., & Hughes, S. A. 1998, PhRvD, 57, 4535
Hurley, J. R., Pols, O. R., & Tout, C. A. 2000, MNRAS, 315, 543
Jiang, C. Y., Jing, Y. P., Faltenbacher, A., Lin, W. P., & Li, C. 2008, ApJ, 675, 1095
Kaaret, P., Feng, H., & Roberts, T. P. 2017, ARA&A, 55, 303
Kızıltan, B., Baumgardt, H., & Loeb, A. 2017, Natur, 542, 203
Kocsis, B., Ray, A., & Portegies Zwart, S. 2012, ApJ, 752, 67
Kocsis, B., Yunes, N., & Loeb, A. 2011, PhRvD, 84, 024032
Konstantinidis, S., Amaro-Seoane, P., & Kokkotas, K. D. 2013, A&A, 557, A135
Kozai, Y. 1962, AJ, 67, 591
Kroupa, P. 2001, MNRAS, 322, 231
Kruijssen, J. M. D., & Lützgendorf, N. 2013, MNRAS, 434, L41
Kushnir, D., Zaldarriaga, M., Kollmeier, J. A., & Waldman, R. 2016, MNRAS, 462, 844
Leigh, N. W. C., Böker, T., Maccarone, T. J., & Perets, H. B. 2013, MNRAS, 429, 2997
Leigh, N. W. C., Lützgendorf, N., Geller, A. M., et al. 2014, MNRAS, 444, 29
Leigh, N. W. C., & Sills, A. 2011, MNRAS, 410, 2370
Lidov, M. L. 1962, P&SS, 9, 719
Lousto, C. O., Campanelli, M., Zlochower, Y., & Nakano, H. 2010, CQGra, 27, 114006
Lousto, C. O., & Zlochower, Y. 2008, PhRvD, 77, 044028
Lousto, C. O., & Zlochower, Y. 2011, PhRvL, 107, 231102
Lousto, C. O., Zlochower, Y., Dotti, M., & Volonteri, M. 2012, PhRvD, 85, 084015
Lützgendorf, N., Baumgardt, H., & Kruijssen, J. M. D. 2013, A&A, 558, A117
Lützgendorf, N., Kissler-Patig, M., Gebhardt, K., et al. 2012, A&A, 542, A129
Lützgendorf, N., Kissler-Patig, M., Gebhardt, K., et al. 2013a, A&A, 552, A49
Lützgendorf, N., Kissler-Patig, M., Neumayer, N., et al. 2013b, A&A, 555, A26
MacLeod, M., Trenti, M., & Ramirez-Ruiz, E. 2016, ApJ, 819, 70
Madau, P., & Rees, M. J. 2001, ApJL, 551, L27
Madrid, J. P., Leigh, N. W. C., Hurley, J. R., & Giersz, M. 2017, MNRAS, 470, 1729
Mandel, I., Brown, D. A., Gair, J. R., & Miller, M. C. 2008, ApJ, 681, 1431

McKernan, B., Ford, K. E. S., Kocsis, B., Lyra, W., & Winter, L. M. 2014, MNRAS, 441, 900
McKernan, B., Ford, K. E. S., Lyra, W., & Perets, H. B. 2012, MNRAS, 425, 460
Merritt, D. 2013, Dynamics and Evolution of Galactic Nuclei (Princeton, NJ: Princeton Univ. Press)
Merritt, D., & Ferrarese, L. 2001, ApJ, 547, 140
Mezcua, M. 2017, IJMPD, 26, 1730021
Miller, M. C. 2002, ApJ, 581, 438
Miller, M. C., & Hamilton, D. P. 2002, MNRAS, 330, 232
Miller, M. C., & Miller, J. M. 2015, PhR, 548, 1
Milosavljević, M., & Merritt, D. 2001, ApJ, 563, 34
Moore, C. J., Cole, R. H., & Berry, C. P. L. 2015, CQGra, 32, 015014
Morscher, M., Pattabiraman, B., Rodriguez, C., Rasio, F. A., & Umbreit, S. 2015, ApJ, 800, 9
Morscher, M., Umbreit, S., Farr, W. M., & Rasio, F. A. 2013, ApJL, 763, 15
Navarro, J. F., Frenk, C. S., & White, S. D. M. 1997, ApJ, 490, 493
O'Leary, R. M., Kocsis, B., & Loeb, A. 2009, MNRAS, 395, 2127
O'Leary, R. M., Meiron, Y., & Kocsis, B. 2016, ApJL, 824, L12
O'Leary, R. M., Rasio, F. A., Fregeau, J. M., Ivanova, N., & O'Shaughnessy, R. 2006, ApJ, 637, 937
Pasham, D. R., Strohmayer, T. E., & Mushotzky, R. F. 2014, Natur, 513, 74
Peters, P. C. 1964, PhRv, 136, 1224
Petts, J. A., & Gualandris, A. 2017, MNRAS, 467, 3775
Planck Collaboration, Ade, P. A. R., Aghanim, N., et al. 2016, A&A, 594, A13
Portegies Zwart, S. 2006, The Ecology of Black Holes in Star Clusters, ed. F. Haardt et al. (Bristol: IOP Publishing), 387
Portegies Zwart, S. F., & McMillan, S. L. W. 2000, ApJL, 528, L17
Portegies Zwart, S. F., & McMillan, S. L. W. 2002, ApJ, 576, 899
Prieto, J. L., & Gnedin, O. Y. 2008, ApJ, 689, 919
Rodriguez, C. L., Morscher, M., Pattabiraman, B., et al. 2015, PhRvL, 115, 051101
Sérsic, J. L. 1963, BAAA, 6, 41
Sesana, A., Sartore, N., Devecchi, B., & Possenti, A. 2012, MNRAS, 427, 502
Shapiro, S. L. 2005, ApJ, 620, 59
Sigurdsson, S., & Phinney, E. S. 1993, ApJ, 415, 631
Sopuerta, C. F., Yunes, N., & Laguna, P. 2007, ApJL, 656, 9
Spitzer, L., Jr. 1969, ApJL, 158, L139
Terzić, B., & Graham, A. W. 2005, MNRAS, 362, 197
Tiongco, M. A., Vesperini, E., & Varri, A. L. 2016, MNRAS, 461, 402
Webb, J. J., Leigh, N., Sills, A., Harris, W. E., & Hurley, J. R. 2014, MNRAS, 442, 1569
Whalen, D. J., & Fryer, C. L. 2012, ApJL, 756, L19
Will, C. M. 2004, ApJ, 611, 1080
Woods, T. E., Heger, A., Whalen, D. J., Haemmerlé, L., & Klessen, R. S. 2017, ApJL, 842, L6
Zaldarriaga, M., Kushnir, D., & Kollmeier, J. A. 2017, MNRAS, 473, 4174